CHEMICAL REVIEWS

Review

pubs.acs.org/CR

Band Bending in Semiconductors: Chemical and Physical Consequences at Surfaces and Interfaces

Zhen Zhang and John T. Yates, Jr.*

Department of Chemistry, University of Virginia, Charlottesville, Virginia 22904, United States

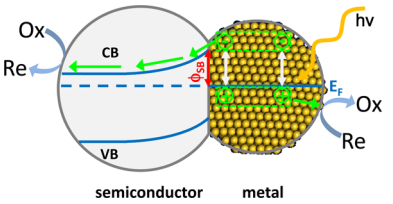

CONTENTS

1. INTRODUCTION

This is the age where the capture of solar energy for useful purposes has gained the attention of the scientific and engineering world. The use of solar energy for the generation of electricity, coupled with its potential to produce fuels from CO_2 waste and H_2O by solar-induced photochemistry, is a goal being pursued worldwide. The optimization of charge transfer processes at semiconductor surfaces by manipulation of the energy bands is therefore a theme of broad generality and current applicability.[1]

The fields of heterogeneous photocatalysis and photochemistry have developed extensively in the past 40 years in response to challenging energy and environmental issues.[2−12] In photocatalysis or photochemistry on surfaces, photon absorption is accompanied by electronic excitation in the substrate or in the adsorbed molecules accompanied by either charge or energy transfer;[6,11] in heterogeneous catalysis, charge transfer can occur independently of any photon excitation. In photocatalysis, the photogenerated charge carrier transfer process between surface and adsorbed molecules constitutes a

Received: February 15, 2012

   dx.doi.org/10.1021/cr3000626 | Chem. Rev. XXXX, XXX, XXX–XXX

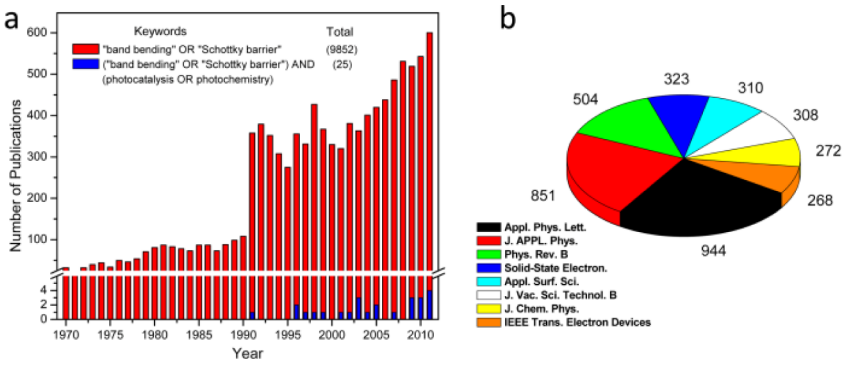

Figure 1. (a) Annual number of papers published in which "("band bending" or "Schottky barrier")" (red) or "("band bending" or "Schottky barrier") and ("photocatalysis" or "photochemistry")" (blue) are the topic words. Pie diagram shows the top eight sources of the papers with the topic word "band bending" or "Schottky barrier". Literature search was done using ISI's Web of Science (www.isiknowledge.com).

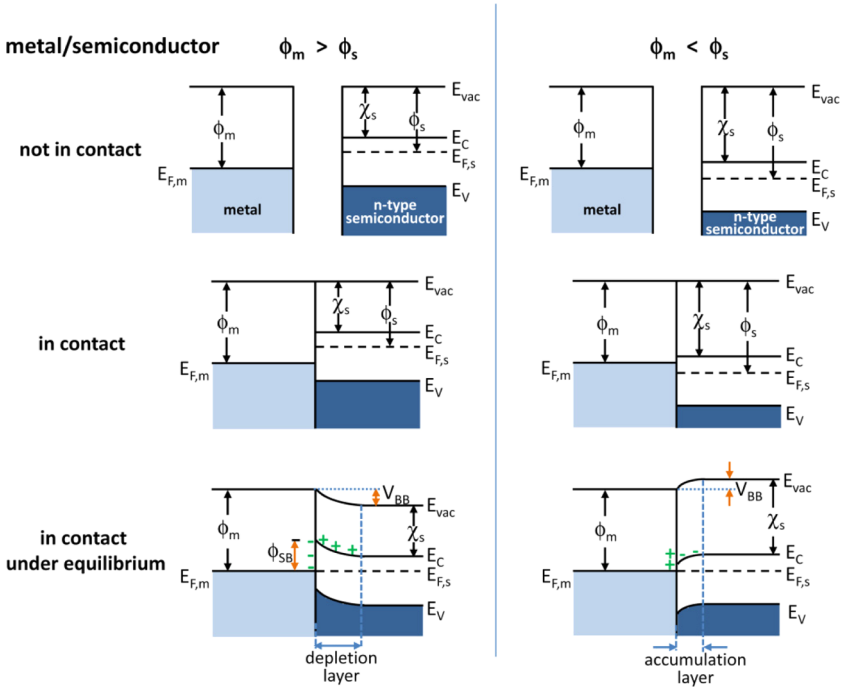

Figure 2. Energy band diagrams of metal and n-type semiconductor contacts. E_{vac}, vacuum energy; E_c, energy of conduction band minimum; E_v, energy of valence band maximum; ϕ_m, metal work function; ϕ_s, semiconductor work function; χ_s, electron affinity of the semiconductor.

complex and fundamental step in chemical processes induced by the absorption of light.

There are over 1000 review papers dealing with the topic of "photocatalysis" or "photochemistry". Most of the review papers are concentrated on some specific area, such as a specific photochemical/photocatalytic process (e.g., photodissociation of H_2O; photochemistry and environmental remediation), photocatalyst preparation or modification, or fabrication of photovoltaic devices. Only rarely do review papers attempt to illuminate the general mechanisms that play important roles in heterogeneous photocatalysis or photochemical processes at surfaces.

In this review, we focus on the principles of band bending and its effect on photochemistry and photocatalysis. This may be helpful to chemists and material scientists in the understanding of the photoexcitation process and the development of highly efficient photoactive materials and processes. The review is divided into three parts dealing with (1) the physical principles of band bending in semiconductors, (2) the measurement of band bending, and (3) the effects of band bending on photochemistry. The band bending concept is of course well established in semiconductor physics[13,14] and has become one of the central concepts in electrochemistry[15−17] and gas sensors.[18,19] As shown in Figure 1, until now, there have been ~10 000 papers with the topic words "band bending" or "Schottky barrier", but most of the papers are in the field of solid state physics, and only 25 papers are found with the words "band bending" together with "photochemistry" or "photocatalysis".

1.1. Band Bending

1.1.1. Metal/Semiconductor Contact Induced Band Bending. The band bending concept was first developed by Schottky and Mott to explain the rectifying effect of metal−semiconductor contacts.[20−23] Figure 2 shows the ideal energy band diagrams of metal and n-type semiconductor contacts. When the metal and semiconductor are in contact, the free electrons will transfer between metal and semiconductor due to the work function difference. If the metal work function (ϕ_m) is

dx.doi.org/10.1021/cr3000626 | Chem. Rev. XXXX, XXX, XXX−XXX

higher than that of the semiconductor (ϕ_s), that is, $\phi_m > \phi_s$ as shown on the left of Figure 2, the electrons will flow from the semiconductor to the metal. The electron transfer will continue until the Fermi levels of metal ($E_{F,m}$) and semiconductor ($E_{F,s}$) are aligned. Under equilibrium, a Helmholtz double layer will be established at the metal/semiconductor interface, where the metal is negatively charged and the semiconductor is positively charged near its surface due to electrostatic induction. Due to the low concentration of free charge carriers in the semiconductor, the electric field between metal and semiconductor interfaces cannot be effectively screened in the semiconductor. This causes the free charge carrier concentration near the semiconductor surface to be depleted compared with the bulk. This region is called the **space charge region**. In the n-type semiconductor (electrons as majority charge carriers), when $\phi_m > \phi_s$, the electrons are depleted in the space charge region, and this region is therefore called the **depletion layer** and is characterized by excess positive charge. When $\phi_m < \phi_s$, as shown in the right side of Figure 2, the electrons are accumulated in the space charge region due to the electron transfer from the metal to the semiconductor, and this region is called the **accumulation layer**. In general, when the Fermi level of the metal is below that of the semiconductor, charge will flow to the metal causing the semiconductor Fermi level to decrease, and vice versa.

In the space charge region, the energy band edges in the semiconductor are also shifted continuously due to the electric field between the semiconductor and the metal due to the charge transfer, which is called **band bending**. The energy bands bend upward toward the interface when $\phi_m > \phi_s$, while the edges bend downward toward the interface when $\phi_m < \phi_s$. One can envision the direction of band bending by thinking about the electrostatic energy experienced by an electron as it moves through the interface. As the electron in the semiconductor experiences repulsion from the negatively charged Helmholtz layer located in the metal, its potential energy rises and the bands bend upward, and vice versa. From Figure 2, compared with the bulk, the degree of bending of the energy band of the semiconductor at the interface equals the work function difference between metal and semiconductor,

$$V_{BB} = |\phi_m - \phi_s| \quad (1)$$

When $\phi_m > \phi_s$ in an n-type semiconductor, there is also a barrier formed at the metal−semiconductor interface, which is called the **Schottky barrier** (ϕ_{SB}),

$$\phi_{SB} = (\phi_m - \chi_s) \quad (2)$$

where χ_s = electron affinity of the semiconductor. When $\phi_m < \phi_s$ in an n-type semiconductor, there is no Schottky barrier and the metal−semiconductor contact is ohmic.

1.1.2. Field-Effect-Induced Band Bending. An external field can also induce band bending near the semiconductor surface. Figure 3 gives a schematic diagram of a field-effect-induced band bending on an n-type semiconductor with no surface states.[24] We assume the work functions of the metal plate and the semiconductor are same for the sake of simplicity. The energy band is flat when the bias voltage between metal and semiconductor is zero ($V = 0$). When a bias voltage is applied to the metal, an electric field is set up between the metal and the semiconductor. The electric field can penetrate into the near surface region of the semiconductor due to the insufficient screening by the charge carriers of low concentration in the semiconductor. When $V > 0$, the electric field causes electron accumulation near the surface and bends the band downward, and vice versa. The field-effect-induced band bending can been measured by surface photovoltage (SPV)[25] and photoluminescence (PL)[26,27] methods.

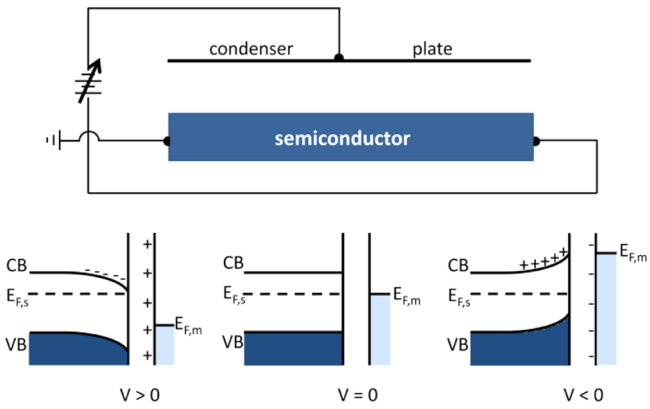

Figure 3. Schematic diagram of field-effect-induced band bending on an n-type semiconductor with no surface states. Adapted with permission from ref 24. Copyright 1956 The Nobel Foundation.

1.1.3. Surface-State-Induced Band Bending. On a clean semiconductor surface, surface states may exist due to the termination of lattice periodicity at the surface. Band bending induced by the surface state is schematically indicated in Figure 4.[28] The unpaired electrons in the dangling bonds of surface atoms interact with each other forming an electronic state with a narrow energy band at the semiconductor band gap. In Figure 4a, we assume the surface state is half filled and centered at the midgap. When the semiconductor is undoped (intrinsic semiconductor), the Fermi level of the bulk (E_F(bulk)) also is located at the midgap and is equal in energy to the surface Fermi level (E_F(surf)). There is no charge transfer between the bulk and the surface, so the bands are flat. If the semiconductor is n-type doped (Figure 4b), E_F(bulk) is closer to the conduction band, which is higher than E_F(surf) under

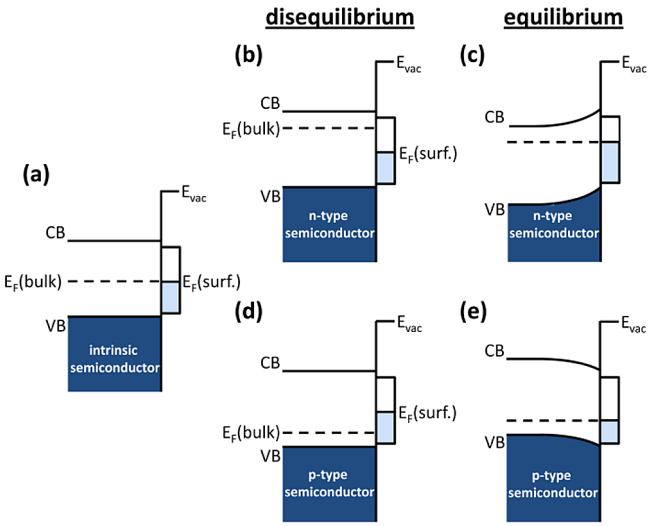

Figure 4. Schematic electron energy levels near the surface of a clean semiconductor: (a) undoped (intrinsic) semiconductor; (b) disequilibrium and (c) equilibrium between n-type bulk and its surface; (d) disequilibrium and (e) equilibrium between p-type bulk and its surface.

dx.doi.org/10.1021/cr3000626 | Chem. Rev. XXXX, XXX, XXX−XXX

disequilibrium. The electrons will transfer from the bulk to the surface. E_F(bulk) drops and E_F(surf) rises until equilibrium is achieved. At equilibrium, the energy bands bend upward as one moves toward the surface (Figure 4c). For a p-type semiconductor, E_F(bulk) is closer to the valence band, which is lower than E_F(surf) under disequilibrium (Figure 4d). The electrons will transfer from the surface to the bulk, causing downward band bending.

Usually, the density of surface states is large ($\sim 10^{15}$ cm^{-2}) in comparison with the bulk dopant states in regions of the bulk semiconductor parallel to the surface ($\sim 10^{8}$–10^{12} cm^{-2}). Therefore, the Fermi level of the semiconductor is almost independent of the bulk dopant concentration and is pinned by the surface states, that is, **Fermi level pinning**. In addition, the presence of a high density of surface (interface) states on the semiconductor surface may screen the influence of the metal/semiconductor contact (section 1.1.1) and field-effect (section 1.1.2) induced band bending. Ionic semiconductors (ZnO, TiO_2, etc.) usually have less density of surface states in the band gap than the covalent semiconductors (Si, GaAs, etc.). Thus, at a metal/ionic semiconductor junction, the contact-induced band bending and Schottky barrier are more dependent on the work function difference in the ionic semiconductor than in the covalent semiconductor.[29]

Obviously, the surface states will be determined by the atomic structure of the semiconductor surface. Consequently, the surface-state-induced band bending may be different on the same semiconductor with a different surface structure, which will be discussed later.

1.1.4. Adsorption-Induced Band Bending. Adsorption on the semiconductor surface can also induce band bending near the surface. Figure 5 shows a schematic diagram of the adsorption of an acceptor molecule (A) on an n-type semiconductor surface.[30] As the molecule approaches the surface, an unfilled molecular orbital interacts with the semiconductor and shifts downward. Meanwhile, the broadened molecular orbital (produced due to the uncertainty principle applied to electron location and energy) accepts electrons from the semiconductor forming a Helmholtz layer on the semiconductor surface. An electric field is set up and the bands are bent upward near the semiconductor surface. For a donor molecule, the electrons will transfer from the molecule to the semiconductor and downward band bending will occur.

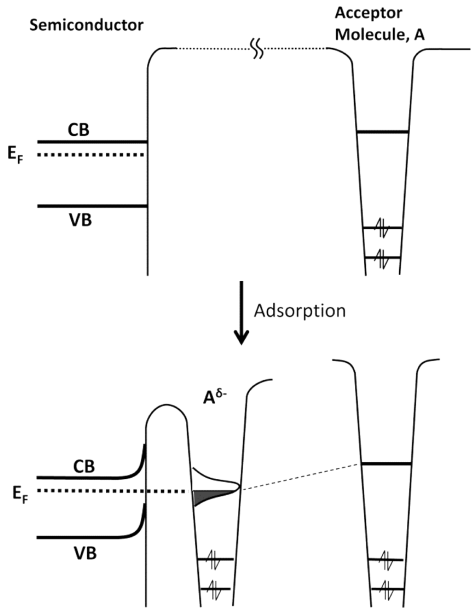

Figure 5. Schematic diagram shows the adsorption of an acceptor molecule (A) on an n-type semiconductor surface with broading of the LUMO level. Reprinted with permission from ref 30. Copyright 2010 American Chemical Society.

1.2. Space Charge Region

Overall, the band bending of a semiconductor in the above-discussed systems is due to the poor screening of the surface charge-induced electric field by the low concentration of free carrier density in the semiconductor. In metals, the free electron density is $\sim 10^{22}$ cm^{-3} with a short screening length on the order of atomic sizes, while the screening length in a semiconductor is on the order of ~100 Å with a free carrier density of $\sim 10^{17}$ cm^{-3}, which creates a space charge region near the semiconductor surface. Physical properties, such as energy band structure, free carrier density, and local conductivity, will also be changed in the space charge region compared with the bulk,[31] and hence the chemical properties will be changed also.

Figure 6 summarizes three kinds of space charge regions schematically.[6,31,32] For simplicity, we use an n-type semiconductor as an example, in which the majority carriers are electrons, that is, the density of free electron carriers (n_e) is higher than that of hole carriers (n_h). There is no space charge in the flat band region. For downward band bending, positive charges exist at the surface and electrons accumulate in the semiconductor near the surface, causing an increase of n_e and a decrease of n_h. This space charge region in the semiconductor is called the **accumulation layer** due to the accumulation of electrons in the semiconductor. In the upward band bending condition, negative charges exist at the surface and positive charges accumulate near the surface, causing a decrease of n_e and an increase of n_h. This space charge region is called the **depletion layer**. In upward band bending, the semiconductor can change to a p-type semiconductor near the surface if the electrons are depleted below the intrinsic level (n_i), i.e., $n_e < n_i < n_h$. For this condition, the space charge region is called the **inversion layer**. It should be mentioned that the amount of charge in the space charge region (Q_{sc}) equals the amount of

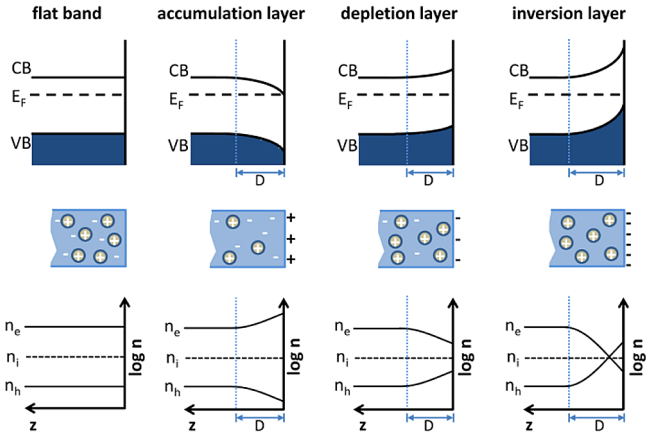

Figure 6. Schematic diagrams showing the energy levels and free charge carrier densities on (logarithmic scale) from the n-type semiconductor surface to the bulk. The blue dotted lines indicate the corresponding space charge region of thickness, D. n_e = free electron density; n_h = free hole density; n_i = intrinsic carrier density.

dx.doi.org/10.1021/cr3000626 | Chem. Rev. XXXX, XXX, XXX–XXX

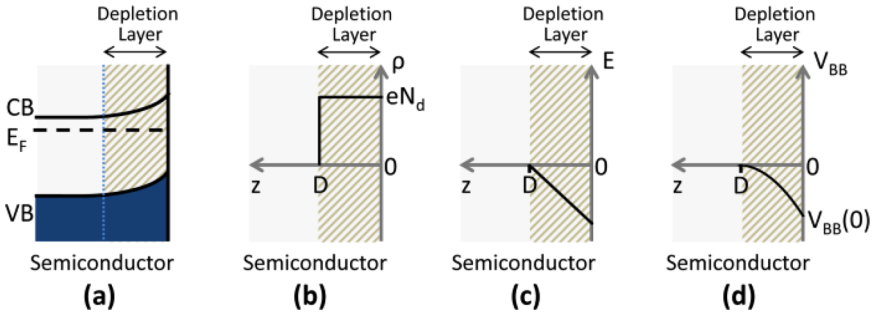

Figure 7. Schematic diagrams of (a) band scheme, (b) space charge density (ρ), (c) electric field (E), and (d) electric potential using the bulk potential as the reference zero point (V_{BB}) of the depletion layer (space charge layer) in an n-type semiconductor in the Schottky approximation. D is the thickness of the depletion layer. Adapted with permission from ref 31. Copyright 2010 Springer Science and Business Media.

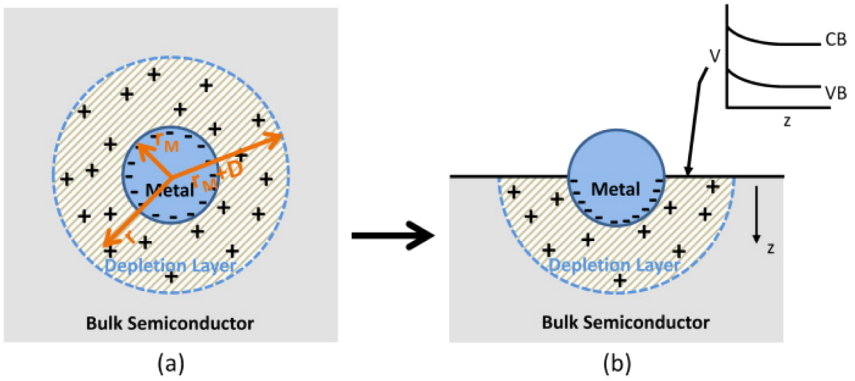

Figure 8. The embedded metal particle model used to simulate the contact of a metal particle with a semiconductor support: (a) semiconductor enclosed metal particle; (b) semiconductor with partially embedded metal particle; inset in panel b, band bending in semiconductor. Adapted with permission from ref 33. Copyright 1996 Elsevier.

surface charge (Q_{surf}) of different polarity due to the charge neutrality, that is,

$$Q_{sc} = -Q_{surf} \tag{3}$$

In the space charge region, the electric potential (V_{BB}) of a point (x, y, z) relative to the bulk of the semiconductor can be described by Poisson's equation,

$$\frac{\partial^2 V_{BB}(x,y,z)}{\partial x^2} + \frac{\partial^2 V_{BB}(x,y,z)}{\partial y^2} + \frac{\partial^2 V_{BB}(x,y,z)}{\partial z^2} = -\frac{\rho}{\varepsilon_r \varepsilon_0} \tag{4}$$

where ρ is the space charge density and ε_r and ε_0 are the relative dielectric constant of the semiconductor and the vacuum permittivity, respectively. In the real situation, ρ is a function of the xyz coordinates and is influenced by the surface charge distribution. To discuss the detailed solution of eq 4 is beyond the scope of this review. Herein, we discuss two simplified models of the metal/semiconductor interface.

1.2.1. Infinite Metal/Semiconductor Interface. Most of the time, the space charge regions that we use to discuss band bending are one-dimensional (e.g., Figures 2–6), which assumes that the surface extends infinitely and surface charges are distributed on the surface homogeneously so that the potential energy of an electron at a certain depth in the semiconductor is invariant in x and y. In this case, V_{BB} is only the function of z (the distance from the surface into the bulk) and does not relate to the x, y coordinates on the surface. Then, eq 4 can be written as

$$\frac{d^2 V_{BB}(z)}{dz^2} = -\frac{\rho}{\varepsilon_r \varepsilon_0} \tag{5}$$

Taking the depletion layer in an n-type semiconductor as an example, for simplicity, two assumptions have been made (Schottky approximation, Figure 7b):[31] (1) In the depletion layer ($0 \ll z \ll D$, D is the depletion layer thickness), the positive charges are due to the completely ionized bulk donors, which are homogeneously distributed with a density of N_d, that is,

$$\rho = eN_d \qquad 0 \le z \le D \tag{6}$$

(2) Beyond the depletion layer, the positive charge is zero, that is,

$$\rho = 0 \qquad z > D \tag{7}$$

From eqs 5–7, the electric field ($E(z)$) and $V_{BB}(z)$ within the space charge region can be obtained,

$$E(z) = \frac{eN_d}{\varepsilon_r \varepsilon_0}(z - D) \quad 0 \le z \le D \tag{8}$$

$$V_{BB}(z) = -\frac{eN_d}{2\varepsilon_r \varepsilon_0}(z - D)^2 \qquad 0 \le z \le D \tag{9}$$

According to eqs 8 and 9, the changes of $E(z)$ and $V_{BB}(Z)$ with the distance z in the space charge region have also been schematically plotted in Figure 7c,d. $E(z)$ changes with z in a linear fashion, while $V_{BB}(z)$ exhibits a parabolic relationship with z. If the band bending value ($V_{BB}(0)$) at the surface (z = 0) is known, the depletion layer thickness, can be obtained

dx.doi.org/10.1021/cr3000626 | Chem. Rev. XXXX, XXX, XXX–XXX

$$D = \left[\frac{2\varepsilon_r\varepsilon_0 V_{BB}(0)}{eN_d}\right]^{1/2} \quad (10)$$

The above infinite metal/semiconductor interface model may be applied when the lateral width of metal/semiconductor interface is higher than the thickness of the space charge region, which is on the order of ~10 nm. However, in the catalytic systems involving small metal and semiconductor particles, most of the metal particles are smaller than 10 nm, which makes it necessary to discuss the finite metal/semiconductor interface model.

1.2.2. Finite Metal/Semiconductor Interface. Ioannides and Verykios[33] proposed a model of an embedded spherical metal particle in a semiconductor, as shown in Figure 8a. Based on the Schottky approximation, the electric field ($E(r)$) and potential ($V_{BB}(r)$) in the space charge region is

$$E(r) = \frac{eN_d}{3\varepsilon_r\varepsilon_0 r^2}[(D + r_M)^3 - r^3]$$

$$r_M \le r \le D + r_M \quad (11)$$

$$V_{BB}(r) = \frac{eN_d}{\varepsilon_r\varepsilon_0}\left[\frac{(D + r_M)^2}{2} - \frac{r^2}{6} - \frac{(D + r_M)^3}{3r}\right]$$

$$r_M \le r \le D + r_M \quad (12)$$

where r is the distance from the center of the metal particle and r_M is the metal particle radius. From eq 12, the contact potential at the metal/semiconductor interface ($V_{BB}(r_M)$) is

$$V_{BB}(r_M) = \frac{eN_d}{\varepsilon_r\varepsilon_0}[\frac{(D + r_M)^2}{2} - \frac{r_M^2}{6} - \frac{(D + r_M)^3}{3r_M}] \quad (13)$$

Equation 13 also indicates that the depletion layer thickness, D, is a function of metal particle radius at fixed $V_{BB}(r_M)$. The depletion layer thickness in the semiconductor was found to decrease with decreasing metal particle size by Smit et al.[34] The comparison of potential profiles of the infinite metal/semiconductor interface model and embedded particle model in the space charge region was investigated by Zhdanov et al.[35]

The above model can be employed to roughly simulate a real metal/semiconductor catalysis system consisting of hemispherical metal particles on a semiconductor oxide surface by removing the upper half of the semiconductor, as shown in Figure 8b, and assuming that the transferred charges between metal and semiconductor in Figure 8b is half of Figure 8a and that most of the charges in the metal locate at the metal/semiconductor interface.[33] It should also be mentioned that the space charge region and band bending may be influenced by the particle shape and charge distribution on the metal particle.[34−39] Figure 8b also shows the local band bending at a point near the metal.

The model in Figure 8 also gives us a clear idea that the space charge region (band bending region) not only distributes itself beneath the metal/semiconductor interface vertically, as was discussed in the infinite metal/semiconductor interface model, but also distributes itself along the semiconductor surface laterally away from the metal, which may influence the chemisorption and reaction of molecules adsorbed near the metal particle. As an example, the space charge region induced by a circular metal disk on a semiconductor has been studied by Donolato.[39] Assuming $N_d = 10^{15}$ cm^{-3}, $\varepsilon_r = 11.7$, and $V_{BB} = 0.4$ V, the boundaries of the space charge region for different sizes of metal disks on silicon have been plotted in Figure 9. The simulation indicates the anisotropy of the space charge region

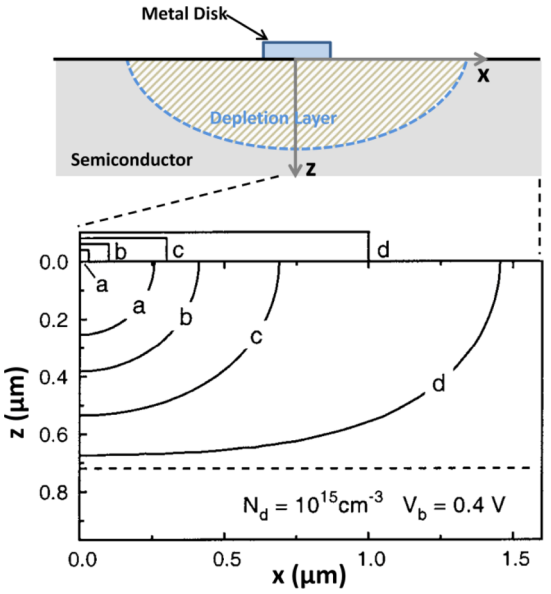

Figure 9. Boundary of the space charge region for different sizes of the disk-shaped Schottky contacts. The values of the disk radius are (a) 0.03, (b) 0.1, (c) 0.3, and (d) 1 μm. The horizontal dashed line represents the space charge boundary position according to the infinite metal/semiconductor interface model. Adapted with permission from ref 39. Copyright 2004 American Institute of Physics.

along the normal (z) and lateral (x) directions of the metal/semiconductor interface. For a small metal disk, the lateral space charge region is comparable to the vertical space charge region, which is smaller than the space charge region (dashed line) in the infinite metal/semiconductor system. As the metal disk size increases, the space charge region in the z direction approaches the dashed line and the space charge region along x direction will become fractionally less predominant. The lateral band bending in this exterior region has also been studied by STM, PES, and SPV methods.[40−43]

1.3. Applications of the Band Bending Concepts

The presence of band bending and the associated electric field in the space charge region can promote not only the separation of electrons and holes, but also the diffusion of charge carriers, such as ions, electrons, and holes. The fields of electrochemistry[15−17] and gas sensors[18,19] extensively employ the concept of band bending. The band bending concept applies to many other fields where dopant ions or partially charged interstitial ions move, as for example in TiO_2 materials containing Ti^{3+} interstitial species.[44−48] Two simple examples are discussed below.

1.3.1. Ion Diffusion in Metal Oxides. Based on measurements of the kinetics of growth of thin oxide films (less than ~10 nm) on metal surfaces due to the oxidation of the metal at low temperature, Cabrera and Mott[49] proposed a mechanism with the following assumptions: (1) electrons can transfer through the thin metal oxide film between metal and adsorbed oxygen atoms/molecules (by tunneling or thermionic emission[50,51]) to maintain the same electrochemical potentials (Fermi levels) of metal and the adsorbed oxygen layer; (2) a strong electric field is set up in the thin metal oxide film between the metal and the adsorbed oxygen layer due to the

dx.doi.org/10.1021/cr3000626 | Chem. Rev. XXXX, XXX, XXX−XXX

electron transfer, which decreases the energy barrier for positive ion diffusion in the oxide film.

As shown in Figure 10,[49,52] the energy bands in the oxide film are bent upward due to the presence of an electric field

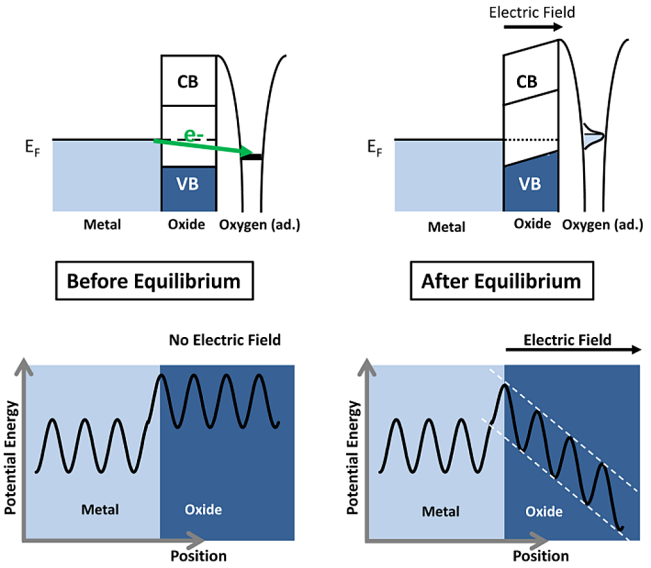

Figure 10. (Upper) Schematic electronic energy levels of metal, oxide, and adsorbed oxygen before and after the establishment of equilibrium of the electrochemical potentials (Fermi levels) between metal and adsorbed oxygen layer. (Lower) Schematic diagrams showing the potential energy of an interstitial metal "positive ion" as a function of position near the metal/oxide interface during thin film growth. The corrugation of the potential energy of the ion is caused by the positively charged lattice cations in the metal and the oxide. The electric field generated by the transfer of electrons from metal to oxygen lowers the energy barriers for ions moving away from the metal/oxide interface toward the surface. Adapted with permission from refs 49 and 52. Copyrights 1949 IOP Publishing Ltd. and 1985 the American Physical Society.

between metal and adsorbed oxygen layer, which is set up by the electron transfer from metal to the adsorbed oxygen layer. The strong electric field of the order of 10^6 V cm^{-1} (assuming 1 V potential difference between metal and adsorbed oxygen and 10 nm thicknesses of oxide film) can promote the positive metal ion diffusion across the oxide film to react with the adsorbed oxygen forming a new metal oxide layer at the **outer** surface. In contrast, the diffusion of negative oxygen ions in the opposite direction from the surface into the interface has also been found in the oxidation of silicon.[53] Thus a metal oxide film grows on the outer surface of the oxide film, but a semiconductor oxide film grows at the inner interface. This difference has been experimentally confirmed in recent multitip STM experiments on Al(111) and Si(100).[53]

From the above discussion on the Cabrera–Mott mechanism, the intensity and direction of the electric field in the oxide film will influence the ion diffusion and the oxidation rate of a metal. For example, an enhanced Al oxidation on Al(111) has been achieved by setting up a strong electric field in the alumina film using electron bombardment.[54] From Figure 2, upward band bending or downward band bending can be obtained by tuning the metal and oxide work functions. By depositing a metal on an oxide surface (which becomes positively charged), Fu et al. found that downward band bending in the oxide promotes outward diffusion of negative oxygen ions in the oxide and favors metal oxidation.[55,56] However, upward band bending in the oxide promotes outward diffusion of positive metal ions in the oxide and favors a metal encapsulation reaction process.[56,57]

1.3.2. Chemicurrent Measurements. The energy transfer or energy dissipation during surface reactions is of fundamental and practical importance in heterogeneous catalysis research. Chemical energy can dissipate through the production of phonons (adiabatically) or the excitation of electrons (non-adiabatically) in the solid.[58,59] Electronic excitations, such as exoelectron emission and chemiluminescence, have been observed for highly exothermic surface reactions.[59−62] However, there was no direct experimental evidence of the reaction-induced excitation of electron−hole pairs on a metal surface until Nienhaus et al. measured a chemicurrent on a metal/semiconductor diode.[59,63,64]

Figure 11a shows schematically the structure of the diode for measuring the excitation of electron−hole pairs by H

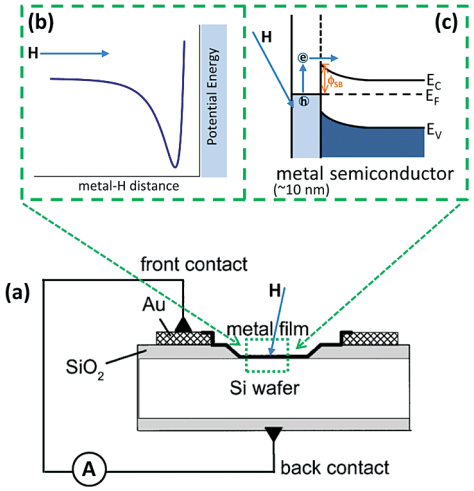

Figure 11. (a) Schematic diagram shows the measurement of chemicurrent produced by H adsorption on metal film. The metal film (~10 nm) is evaporated on an n-type Si wafer forming a Schottky diode. The chemicurrent between metal and n-Si due to H adsorption can be detected by an ammeter. (b) One-dimensional potential energy curves for H adsorption on the metal surface. Metal is on the right side. (c) Principle of chemicurrent production. H atoms react with the metal surface creating e−h pairs. The hot electrons travel ballistically through the film into the semiconductor. Adapted with permission from ref 63. Copyright 1999 the American Physical Society.

adsorption on a metal surface.[63] A metal film (~10 nm) is evaporated on n-type Si. At the metal/n-Si interface, a space charge layer forms and energy bands bend upward forming a Schottky barrier, ϕ_{SB}. The adsorption of H atoms on Ag and Cu has been measured. The adsorption of H on the metal surface is exothermic by ~2.5 eV, and the liberation of this energy excites the electrons in the metal. The electrons with energy higher than ϕ_{SB} can cross the barrier and transfer to the Si. (The thin metal film with thickness of less than ~10 nm guarantees the transfer of ballistic electrons from the H/metal surface to the metal/semiconductor interface.) The rate of electron transfer, the chemicurrent, can be measured between the metal film and Si substrate. In the study of Mg oxidation on Mg/p-Si(111) diodes, Glass and Nienhaus[65] reported that the chemicurrent directly represents the oxidation reaction rates on the metal surfaces. Steady-state chemicurrent produced by

dx.doi.org/10.1021/cr3000626 | *Chem. Rev.* XXXX, XXX, XXX−XXX

heterogeneous catalytic reactions on metal/semiconductor diodes has also been achieved and used by the Somorjai group to study the fundamental issues in catalysis.[66−71] It should be cautioned that Creighton and Coltrin[72] recently argued that the reaction-induced current is generated from a thermoelectric voltage and not from the electron−hole excitation, calling into question the existence of the chemicurrent phenomena.

2. MEASUREMENTS OF BAND BENDING AT SEMICONDUCTOR SURFACES

2.1. Photoelectron Spectroscopy (PES)

Photoelectron spectroscopy is one of the most widely used methods to measure band bending in semiconductors.[73−75] An energy diagram for a photoemission process is shown in Figure 12. According to the photoelectric effect principle, electrons in

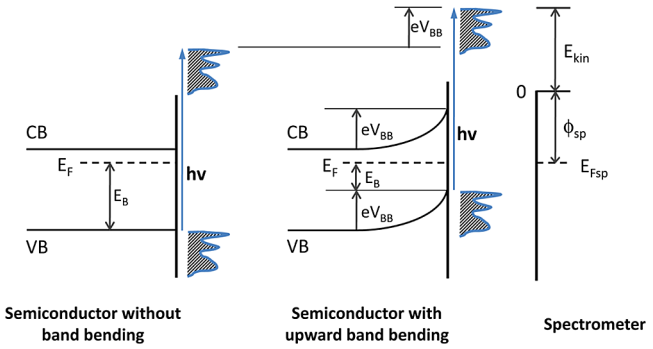

Figure 12. An energy diagram of a photoemission process for a semiconductor.

the sample with a binding energy E_B relative to the Fermi level can be excited from the semiconductor surface by the absorption of photons with energy $h\nu$. The emitted electrons can be accelerated or decelerated by an external electric field due to the work function difference between the sample and spectrometer, which are electrically connected in order to equalize the Fermi levels. The kinetic energy (E_{kin}) of the emitted electrons entering the spectrometer is measured by an energy analyzer. Then, the binding energy, E_B, can be calculated from the energy conservation law, $E_B = h\nu - E_{kin} - \phi_{sp}$, where ϕ_{sp} is the work function of the spectrometer. Figure 12 shows an energy level diagram where the magnitude of the band bending, eV_{BB}, is measured in the shift of a photoemission spectrum from the valence band of electronic states to higher kinetic energy (E_{kin}) relative to the vacuum level. For downward band bending, the shift will be in the opposite direction. This diagram is technically only correct if the atoms undergoing the photoemission process are located at the surface of the semiconductor where the band energy is defined. Since the emission of photoelectrons occurs from the near surface regions, which include subsurface atoms, the argument of Figure 12 is not exact since band bending effects below the surface will vary with photoelectron sampling depth. The variable degree of band bending over the sampled region of the surface will broaden the measured energy distribution.

Depending on the energy of the incident photons, the PES is designated X-ray photoelectron spectroscopy (XPS) using X-ray photon energies in the approximate range of 200−2000 eV or ultraviolet photoelectron spectroscopy (UPS) using ultraviolet photon energies in the approximate range of 10−45 eV.

Taking $O_2/TiO_2(110)$ as an example, it has been reported by several groups[44,76−78] that the adsorption of the electron acceptor molecule, O_2, will lead to transfer of electrons from the $TiO_2(110)$ substrate, causing the energy bands to bend upward. Using ambient-pressure XPS (APXPS), Porsgaard et al.[77] found that exposure to O_2 induces a shift of both the Ti 2p and the O 1s peaks toward lower binding energy as shown in Figure 13. The maximum binding energy shift is ~0.4 eV with

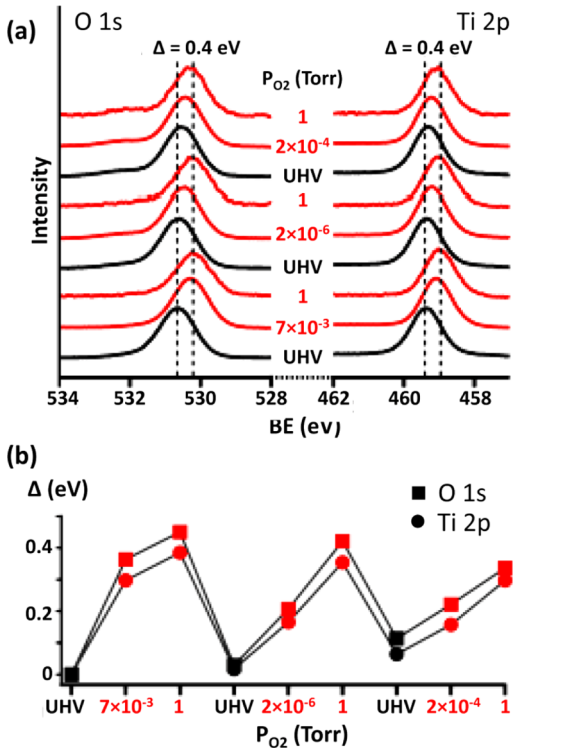

Figure 13. (a) Series of O 1s and Ti 2p spectra measured on $TiO_2(110)$ for different pressures of O_2. The spectra acquired in UHV (black lines) are the first in the series. The spectra are shown offset for clarity. (b) Shifts in the peak position relative to the positions in the first spectrum. Reprinted with permission from ref 77. Copyright 2011 John Wiley and Sons Ltd.

an ambient oxygen pressure of 1 Torr at room temperature. The upward band bending is reversible and can be diminished by desorbing O_2 at room temperature.

In PES experiments, special attention must be paid to surface photovoltage effects caused by the photons and the redistribution of charge in the surface region.[79] In addition, chemical reactions at the surface possibly also caused by radiation damage can cause chemical shifts that are not related to band bending.[80,81] There are several derivative PES methods such as two-photon photoemission (2PPE) spectroscopy[82,83] and inverse photoemission spectroscopy (IPES)[84,85] that can also be used to measure band bending.

2.2. Photoluminescence (PL) Spectroscopy

As a contactless and nondestructive method, photoluminescence spectroscopy is widely used in studying the electronic structures and chemical processes in semiconductors.[86−90] Figure 14 shows a typical experimental setup for PL measurements.[88] Ordinary PL equipment consists of an optical source (monochromated lamp or laser source) as an excitation source and an optical power meter or spectrophotometer to measure the PL intensity. When the semiconductor surface is

dx.doi.org/10.1021/cr3000626 | Chem. Rev. XXXX, XXX, XXX−XXX

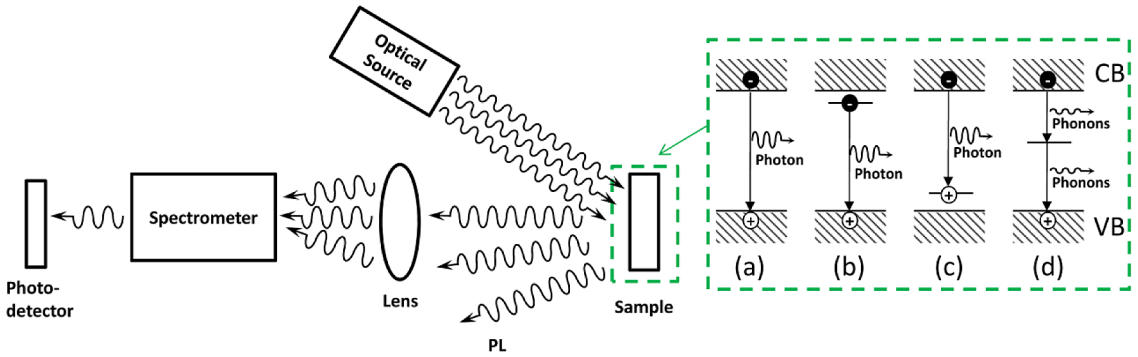

Figure 14. Schematic diagram of the typical experimental setup for photoluminescence (PL) measurements and mechanisms. (a–c) Radiative recombination paths: (a) band-to-band; (b) electron-trap state to valence band; (c) conduction band to hole-trap state. (d) Nonradiative recombination via an intermediate state, emitting phonons to the lattice. Adapted with permission from ref 88. Copyright 2000 John Wiley and Sons Ltd.

illuminated by light with sufficient energy above the bandgap, photons are absorbed strongly. Electrons are excited from the valence band to the conduction band, leaving a hole in the VB. The electron and hole can recombine by a direct band-to-band recombination mechanism by emitting a photon (Figure 14a). In the semiconductor, there are some defects or impurities, which may act as electron or hole traps. The photon-excited electron or hole may also be trapped at these trap states (electron trap, Figure 14b, or hole trap, Figure 14c) and then recombine with a hole usually at the top of the valence band thereby emitting a photon. The deeper trap states tend to facilitate nonradiative recombination by emitting phonons (Figure 14d). The trap-assisted recombination (cases b and c) is also called Shockley–Read–Hall (SRH) recombination.[91–93]

PL can be used as a measurement of band bending.[94–99] The influence of the adsorption of O_2 and 1-C_4H_8 on the PL intensity of n-type (upward band bending) TiO_2 has been investigated by Anpo et al.[95] as shown in Figure 15. A PL feature band at 450–550 nm (2.8–2.3 eV) was found for a TiO_2 sample when excited with 300 nm light (4.1 eV), which is larger than the bandgap of TiO_2 (~3.1 eV). The lower PL photon energy, compared with the bandgap energy of TiO_2, indicates that the electron–hole pair may recombine via the trap states within the forbidden gap by the SRH mechanism. The left part of Figure 15 shows that the adsorption of O_2 decreases the PL intensity. Only 15% of the PL remains unquenched under 1 atm of O_2, and PL cannot be quenched further with more oxygen. This observation may indicate that the luminescence quenching effects by the triplet O_2 itself may not apply. A similar result has also been found for N_2O adsorption. In contrast, the adsorption of the electron-donor 1-C_4H_8 molecule increases the PL intensity. The adsorption of other unsaturated hydrocarbons (C_3H_6, $C_2H_5C{\equiv}CH$, $CH_3C{\equiv}CH$, C_2H_4, $CH{\equiv}CH$), H_2O, and H_2 also enhanced the PL intensity. Further study indicated the PL intensity strongly depended on the ionization potential of the adsorbed molecules: the lower the ionization potential of the added molecule, the larger the increase of PL intensity.

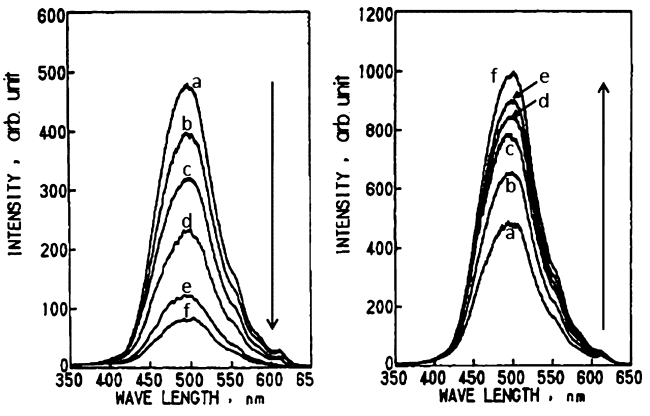

Figure 15. (left) PL spectra of n-type TiO_2 powder at 77 K in the absence (spectrum a) and presence of added O_2 (spectra b–f). Excitation wavelength = 300 nm; temperature = 77 K; amounts of added O_2 (in 10^{-6} mol/g of catalyst): (a) 0; (b) 1.1; (c) 4.7; (d) 11.8; (e) 38.2; (f) 72–150. (right) PL spectra of n-type TiO_2 at 77 K in the absence (spectrum a) and presence of added 1-C_4H_8 (spectra b–f). Excitation wavelength = 300 nm; temperature = 77 K; amounts of added 1-C_4H_8 (in 10^{-6} mol/g of catalyst): (a) 0; (b) 4.7; (c) 16.2; (d) 25.7; (e) 38.2; (f) 72–148. Reprinted with permission from ref 95. Copyright 1989 American Chemical Society.

The above results can be explained qualitatively by the dead-layer model.[95–100] The dead layer is roughly equivalent to the depletion region near the surface caused by the band bending. In this region, the near-surface electric field facilitates the spatial separation of photogenerated electron–hole pairs and depresses their recombination rate. Therefore, there is little PL intensity coming from the depletion region (dead layer). The PL intensity (I_{PL}) is determined by the equation[97,98]

$$I_{PL} \propto I_0 \exp(-\alpha D) \tag{14}$$

where I_0 is the incident light intensity, α is the sum of the absorptivities of the incident and emitted phonons, and D is the length of the depletion region. Figure 16 shows the effect of donor and acceptor adsorbed molecules on an n-type semiconductor with upward bent bands. In this case, the donor and acceptor molecules have an opposite effect on the intensity of PL. For a semiconductor with a flat band, donor and acceptor molecules will have the same effect on the intensity of photoluminescence, causing a reduction in PL intensity, since in the case of either positive or negative band bending from the flat band, the depth of the active PL region will decrease. As shown in Figure 16, the adsorption of O_2 or N_2O (electron acceptor molecules) causes transfer of electrons from the TiO_2 to the adsorbed molecule, bending the energy band upward by the formation of negatively charged species on the surface. In contrast, the electron donor molecules (such as

dx.doi.org/10.1021/cr3000626 | Chem. Rev. XXXX, XXX, XXX–XXX

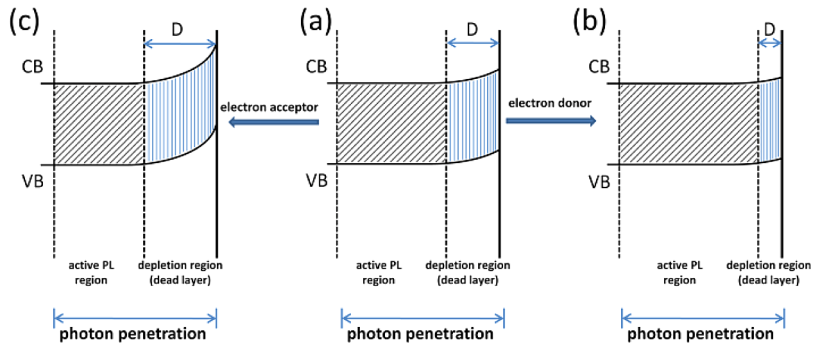

Figure 16. Schematic description of the surface band bending of TiO_2: (a) after cleaning in vacuo (n-type semiconductor); (b) after adsorption of electron donor molecules (1-C_4H_8, C_3H_6, $C_2H_5C{\equiv}CH$, $CH_3C{\equiv}CH$, C_2H_4, $CH{\equiv}CH$, H_2O, H_2) causing a decrease of band bending by formation of positively charged species on the surfaces; (c) after adsorption of electron acceptor molecules (O_2, N_2O) causing a increase of band bending by formation of negatively charged species on the surfaces. The intensity of PL varies as the thickness of the active region varies due to band bending. Adapted with permission from refs 96 and 98 Copyrights 1991 the Chemical Society of Japan and 1988 American Chemical Society.

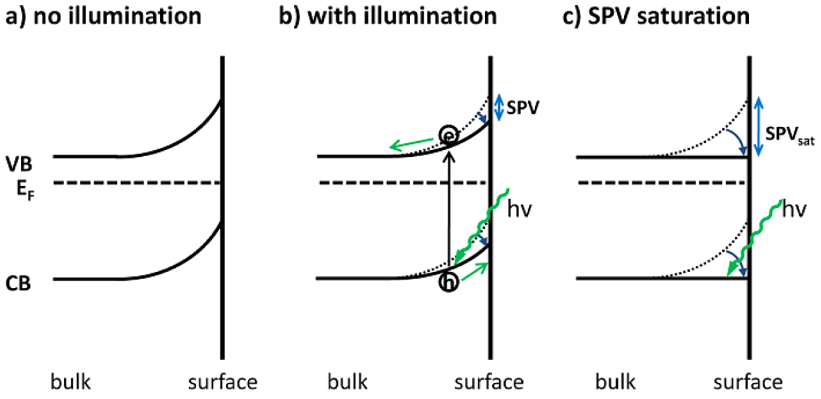

Figure 17. Schematic diagrams of the surface photovoltage effect. (a) Upward band bending in n-type semiconductor; (b) absorbed photons produce free charge carriers resulting in a partial band flattening; (c) largest possible SPV (saturation SPV) occurs to completely flatten bands. Reprinted with permission from ref 103. Copyright 2010 John Wiley and Sons Ltd.

1-C_4H_8) decrease the upward band bending in the n-type TiO_2. From eq 10, the length of the depletion region (dead layer) is proportional to the square root of the magnitude of the band bending. Increased upward band bending by the adsorption of an electron acceptor molecule will increase the dead layer length D, thus decreasing the length of the active PL region and the PL intensity. On the other hand, a decrease of dead layer length on an n-type semiconductor by the adsorption of electron donor molecules enhances the PL intensity.

According to the dead layer model, the change of the length of the depletion/dead layer can be quantitatively measured by monitoring the change of the PL intensity. The ratio of the PL intensity of the clean TiO_2 (I_{PL1}) to the adsorbate-covered TiO_2 (I_{PL2}) is

$$I_{PL1}/I_{PL2} = \exp(-\alpha \Delta D) \quad (15)$$

where ΔD is the corresponding change of the dead layer thickness after the adsorption of electron acceptor or donor molecules. Using this model, Meyer et al.[98] quantitatively analyzed the amine-induced band bending on n-CdSe.

2.3. Surface Photovoltage (SPV) Measurements

The SPV is defined as the illumination-induced change in the surface potential, which was first studied by Brattain and Bardeen.[101,102] A simplified schematic mechanism is indicated in Figure 17.[103] Taking an n-type semiconductor as an example, the energy bands bend upward at the surface (Figure 17a), which may be caused by Fermi level pinning of surface states or by the presence of defects such as oxygen vacancies in TiO_2, imparting negative charge to the surface. As discussed in section 1.1, an electric field will be established near the semiconductor surface due to incomplete screening of the surface charge. The absorption of UV photons with energy higher than bandgap energy creates electron−hole pairs via a band-to-band transition as shown in Figure 17b. (For simplification, trap-to-band transitions will not be discussed here.)[104] The electron−hole pairs will separate as the produced free charge carriers move in different directions due to the near-surface electric field in the bent-band region. Free electrons transfer to the bulk and free holes move to the surface causing a partial band flattening as excess negative charge is neutralized there. The SPV value is determined by measuring the change of the surface potential (V_s) before and after illumination, which can be written SPV = V_s(illumination) − V_s(dark). For a semiconductor with upward bent bands, irradiation will cause the band to flatten as the negative surface charge decreases as a result of hole transport to the surface. The opposite occurs for the semiconductor with downward bent bands; upon irradiation the surface becomes more negatively charged, causing the degree of downward band bending to decrease. For increasing photon flux, the energy bands may be completely flattened (Figure 17c) and the saturated SPV (SPV_{sat}) value is equivalent to the initial magnitude of band bending of the semiconductor. The surface potential change due to the SPV can be measured by the Kelvin

dx.doi.org/10.1021/cr3000626 | Chem. Rev. XXXX, XXX, XXX−XXX

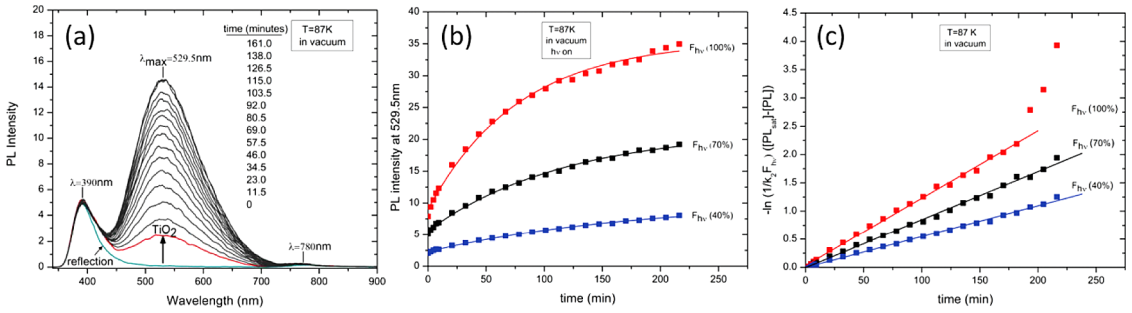

Figure 18. (a) Development of photoluminescence spectrum of TiO_2 in vacuum due to UV irradiation in vacuum. (b) Photoluminescence intensity of TiO_2 as a function of time at different photon fluxes: 100%, 70%, and 40% of 1.5×10^{14} photons cm^{-2} s^{-1}. The rate of production of photon-accessible defect concentration decreases as the light intensity decreases. $h\nu_{excitation}$ = 3.88 eV; $h\nu_{PL}$ = 2.34 eV. (c) Functional fit of PL intensity development during irradiation for different photon fluxes: $F_{h\nu}$ = 100%; $F_{h\nu}$ = 70%; $F_{h\nu}$ = 40%. Solid squares represent experimental data. All data in panels b and c are fitted by eq 16 and fits are shown by solid lines. Reprinted with permission from ref 99. Copyright 2012 American Chemical Society.

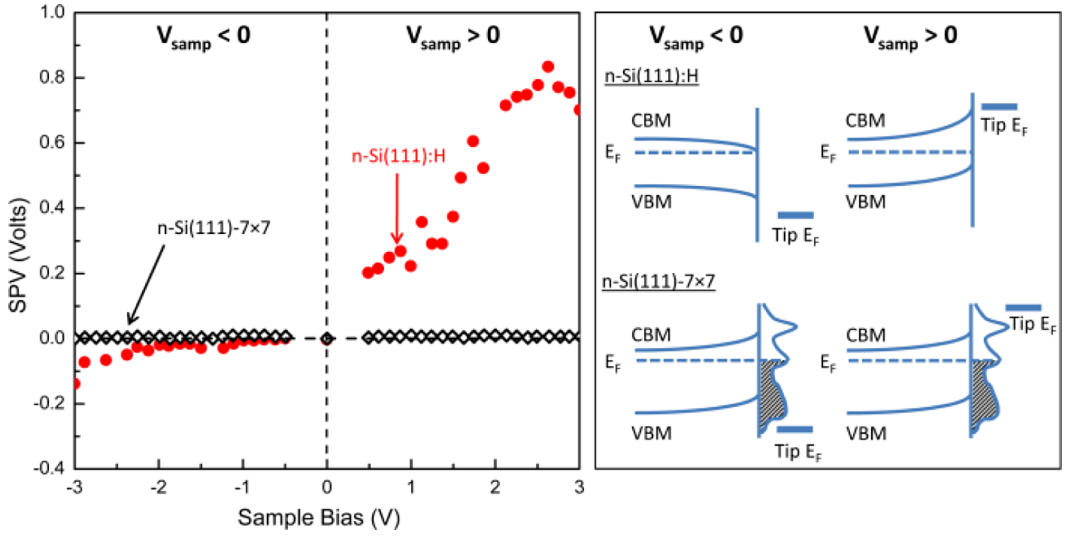

Figure 19. (left) Saturated surface photovoltage vs sample bias (V_{samp}) at 0.3 nA tunneling current for n-type Si(111)-7 × 7 and H-terminated Si(111) (Si(111):H) surfaces. (right) Schematic illustration of tip-induced band bending for n-type H-terminated Si(111) and Si(111)-7 × 7 for $V_{samp} < 0$ (left) and $V_{samp} > 0$ (right). Reprinted with permission from ref 25. Copyright 1993 the American Physical Society.

probe[104,105] or the capacitive pick-up techniques,[104] as well as photoluminescence.[99]

Figure 18a,b shows the effect of the increase of positive surface potential causing the intensity of PL of TiO_2 to increase due to UV irradiation of an n-type TiO_2 powder.[99] UV light of energy 3.88 eV is incident on the TiO_2 with a flux of 1.5×10^{14} photons cm^{-2} s^{-1}. As negative charge is removed from the surface, the photoluminescence intensity rises. The rate of increase in photoluminescence is given by

$$\text{Rate of PL} = k_2 F_{h\nu}[D_{sat}] - k_2 F_{h\nu}\, e^{-k_1 F_{h\nu} t} \qquad (16)$$

where k_2 is the proportionality constant for PL from $F_{h\nu}$ (the flux of exciting UV light). $[D_{sat}]$ is the maximum concentration of active recombination sites in the region probed by the exciting photons under the flat-band condition when the PL intensity maximizes. The rate constant, k_1, corresponds to the rate of photoproduction of photoactive defect sites, which originally existed as inactive sites for electron−hole pair recombination in the depletion region. These sites become active for recombination as a result of flattening the bands due to the change in the surface photovoltage. Figure 18b,c shows the fit to this model of the experimental behavior of the PL intensity as a function of irradiation time.

Using the SPV method, McEllistrem et al.[25] first quantitatively measured the perturbation of the electronic band structure on n-type Si(111)-7 × 7 and H-terminated Si(111) (Si(111):H) surfaces caused by the electric field of a STM tip. The left part of Figure 19 shows the variation of the saturated SPV as a function of applied voltage between sample and the STM tip. The SPV strongly varied with sample bias (V_{samp}) for Si(111):H but exhibited almost no change for clean n-Si(111)-7 × 7. The schematic mechanism of tip-induced band bending is shown in the right part. For the Si(111):H surface, there are no surface states in the bandgap, and the Fermi level is unpinned.[106] The electric field from the STM tip can penetrate into the subsurface region inducing band bending. For $V_{samp} < 0$, the SPV decreases, which means the positively charged tip induces downward band bending. For $V_{samp} > 0$, the SPV increases above zero, which means that the negatively charged tip induces upward band bending. At V_{samp} = 0, the SPV is zero, which indicates that Si(111):H itself is a flat-band semiconductor. For the n-Si(111)-7 × 7 surface, there is a very high local density of states throughout the gap, which strongly pins the Fermi level near midgap,[107] which will screen

dx.doi.org/10.1021/cr3000626 | Chem. Rev. XXXX, XXX, XXX−XXX

the electric field induced by the tip. So the SPV is independent of the sample bias for the n-Si(111)-7 × 7 surface. The SPV is actually always slightly positive due to slight band bending in the n-type Si(111)-7 × 7.

The oxygen chemisorption effect on the band structure of a TiO_2 film has also been investigated by SPV spectroscopy as shown in Figure 20.[108] A Kelvin probe was used to monitor the surface potential. The maximum SPV generated by exposure to UV light above the bandgap energy on the oxidized sample is ~340 mV, while that of the reduced sample is only ~90 mV. This indicates that the upward surface band bending is much stronger in the oxidized TiO_2 films than in the reduced film, which is attributed to the adsorption of oxygen ions during the annealing in air.

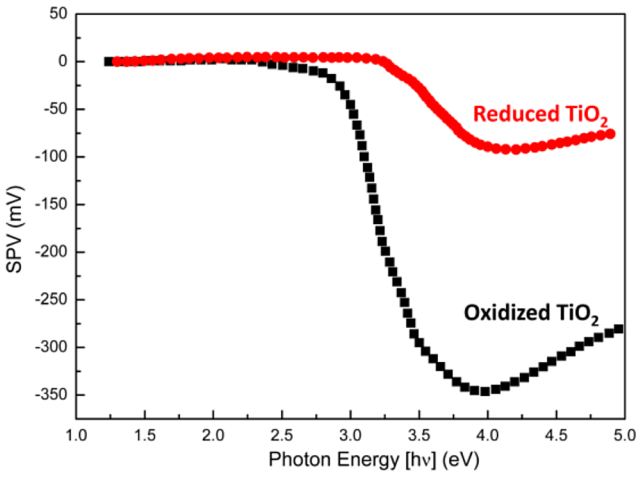

Figure 20. SPV spectra of two TiO_2 samples reduced by annealing in high vacuum (reduced) or oxidized by annealing in atmospheric air (oxidized). Adapted with permission from ref 108. Copyright 2003 Elsevier.

The measurement of the SPV effect can also be combined with other methods, such as photoreflectance (PR) to measure the band bending.[109−111] When the surface band bending changes, the near-surface electric field is changed and will alter the dielectric function. The dielectric function change can be measured by the PR change for light frequencies near the bandgap energy.[110,111] Thus photoreflectance spectroscopy with a modulated laser beam having a photon energy greater than the bandgap energy of the semiconductor can be used to measure band bending.

2.4. Scanning Probe Microscopy (SPM) and Related Methods for Band Bending Measurements

The methods discussed in sections 2.1−2.3 are macroscopic methods for observing average electrical effects over an extended surface region. Compared with other methods, SPM and related methods can be used to measure band bending with atomic resolution. In this section, we will introduce some of the methods, such as scanning tunneling microscopy (STM), scanning tunneling spectroscopy (STS), local barrier height (LBH), and ballistic electron emission microscopy (BEEM) methods, which are influenced by band bending effects.

2.4.1. STM and STS. All the methods we discussed above measure band bending from the bulk to the surface. With STM, band bending as a function of lateral resolution can be measured along the surface.[42,112,113] Figure 21a shows an empty state STM image of a hydrogen-terminated Si(100)-2 × 1 surface (Si(100):H) with a 14 nm $TiSi_2$ island (bright region). It can be seen that a notable "depression" around the $TiSi_2$

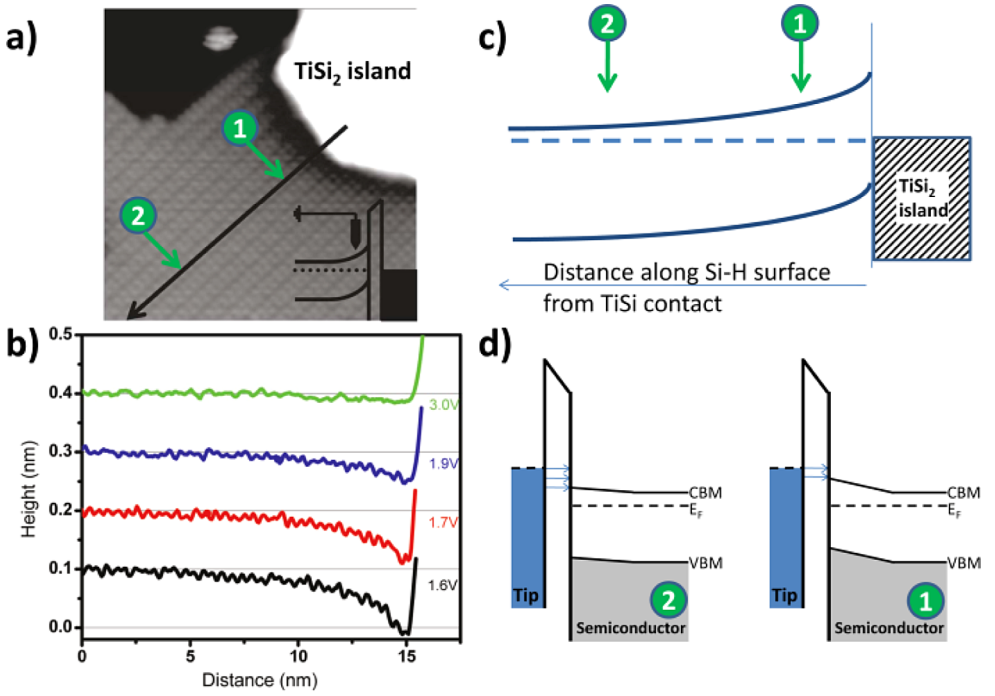

Figure 21. (a) STM image (1.6 V, 60 pA) of the Si(100):H surface surrounding a small $TiSi_2$ island. The silicon surrounding the $TiSi_2$ appears darkened. (b) Line profiles of the silicon surface collected at various voltages. Higher voltages reveal less depression in the silicon. (c) The band diagram illustrates the band bending along the silicon surface, from the titanium silicide contact. (d) Schematic diagram shows the upward band bending at positions 1 and 2 and the STM measurement of empty state imaging. Reprinted with permission from ref 42. Copyright 2011 American Chemical Society.

dx.doi.org/10.1021/cr3000626 | Chem. Rev. XXXX, XXX, XXX−XXX

island is observed on the Si(100):H surface. The line profiles at various sample bias voltages (Figure 21b) show that the depth and length of the depression can change with the applied sample bias and are more notable at low bias voltage. At higher bias voltage, the depression almost disappears due to tip-induced band bending as discussed in section 2.3. The depression is much deeper close to the $TiSi_2$ island. At point 1, which is close to the $TiSi_2$ island, the energy band bends upward more than at point 2 (Figure 21c). If we keep the bias voltage and tip−sample distance constant, the probability of electron tunneling from the STM tip at point 1 is less than at point 2. Consequently, in the constant current STM image, point 1 is much darker than point 2. From the brightness of the STM image, the band bending and spatial distribution of surface charge can be easily measured.

I−*V* spectra have also been acquired at various distances to the $TiSi_2$ island as shown in Figure 22. The black, red, and

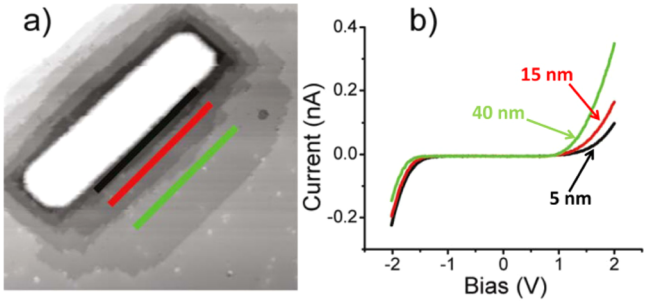

Figure 22. (a) STM image of a $TiSi_2$ island on hydrogen-terminated Si(100). The black, red, and green bars indicate the regions where the corresponding spectra (b) were collected. Ten measurements were averaged for each of the three spectra. A shift of the *I*−*V* spectra is observed due to the surface band bending induced by the $TiSi_2$ island. Reprinted with permission from ref 42. Copyright 2011 American Chemical Society.

green *I*−*V* spectra in Figure 22b are the averages of 10 individual spectra taken at an average distance of 5 nm (black line), 15 nm (red line), and 40 nm (green line) from the $TiSi_2$ island. It can be seen that there is a shift of the spectra of both the filled state and unfilled state region to higher bias voltage at the closer distance to the $TiSi_2$ island. This gives direct evidence, as suggested in Figure 21c, that the upward band bending is more notable on the Si(100):H surface close to the $TiSi_2$ island.

2.4.2. Local Barrier Height (LBH) Measurement. Using the STM to measure the local barrier height,[114−118] one can measure the local work function change on a semiconductor surface caused by band bending. The local tunneling barrier height (LBH) is described by

$$\mathrm{LBH} = \frac{\hbar^2}{8 \times 10^{-20} me}\left(\frac{\mathrm{d} \ln I}{\mathrm{d}z}\right)^2 \approx 0.95\left(\frac{\mathrm{d} \ln I}{\mathrm{d}z}\right)^2 \qquad (17)$$

where $\hbar$ is the reduced Planck constant (1.05×10^{-34} J s), m the electron mass (9.11×10^{-31} kg), I the tunneling current (A), z the tip−sample distance (Å), and LBH (V) is approximately the mean work function of the tip and sample $(\phi_{tip} + \phi_{sample})/2$. During the LBH experiment, the tip−sample distance was modulated sinusoidally and the tunneling current response was measured by a lock-in amplifier. ϕ_{tip} is a constant during the measurement, so the change of LBH is equal to the half of the change of ϕ_{sample}.

The STM and LBH images of Au particles deposited on a $TiO_2(110)$-(1×2) surface were obtained simultaneously by Maeda et al.[119] as shown in Figure 23. Au particles with height from 0.1 to 1.0 nm were observed on cross-link sites of $TiO_2(110)$-(1×2) by STM (Figure 23a). From the LBH image, the large Au particles (indicated by the black arrow) are much brighter than the small particles (indicated by the white arrow). The relative LBH values (ΔLBH) of Au particles to the TiO_2 substrate are plotted as a function of particle height in Figure 23c. The ΔLBH values increased with the particle height. For small particles (particle height <0.4 nm), the values of ΔLBH are mainly distributed from −0.4 to 0 eV, which indicates that the small Au particles may donate electrons to TiO_2 forming a positively charged Au particle. For large particles (particle height >0.4 nm), the values of ΔLBH are distributed from 0 to 0.8 eV, which indicates that the large particles may accept electrons from the TiO_2 forming a negatively charged Au particle. The bandgap obtained from STS (Figure 23d) shows that the size-dependent charge transfer on the TiO_2 surface may due to the metal−nonmetal transition at a critical Au island height of 0.4 nm. The production of $Au^{+0.3}$ single atoms on $TiO_2(110)$ has been verified by O_2 photodesorption measurements and DFT calculation.[120]

2.4.3. Ballistic Electron Emission Microscopy (BEEM). Based on STM, BEEM was invented by Kaiser and Bell in 1988[121,122] to investigate interface band bending in the subsurface region. Figure 24 shows the schematic diagram of the principle of BEEM on the surface of a metal/semiconductor planar structure. In contrast to traditional STM, an additional ammeter is connected to the subsurface semiconductor located adjacent to a metal overlayer in addition to the one connecting the tip, which makes it possible to measure the total tunneling current (I_t) from the tip to a metal/semiconductor sample and the partial tunneling current (I_c) to the buried semiconductor simultaneously. In traditional STM, a bias voltage is applied between the STM tip and metal surface. A total tunneling current (I_t) can be detected originating from the overlap of wavefuntions of the tip and metal surface. Figure 24b shows a schematic diagram of the tunneling from the STM tip to the metal/semiconductor surface. (In this case, we assume a Schottky barrier formed at metal/semiconductor interface.) During the experiment, the ballistic electrons are emitted from the STM tip into the metal/semiconductor structure via vacuum tunneling. The ballistic electrons propagate through the metal layer and reach to the metal/semiconductor interface if the thickness of the metal layer is below the attenuation length of low-energy ballistic electrons (~100 Å[123]). For a sample bias higher than the Schottky barrier, the electrons can cross the barrier and tunneling occurs into the semiconductor as indicated by the green arrow in Figure 24b. The tunneling current from the metal to the semiconductor can be measured using the ammeter between the metal and semiconductor as indicated by Figure 24a. As the tip bias is decreased, bringing E_F to the top of the Schottky barrier, the tunneling current will decrease to zero.

Figure 24c shows the BEEM spectra of the semiconductor current (I_c) vs bias voltage (V) of a Au/Si(100) sample with different total tunneling current (I_t).[121] Irrespective of I_t, I_c is zero at low bias voltage and the onset of current appears at the bias voltage of 0.92 V. That indicates the Schottky barrier height at the Au/Si(100) interface is 0.92 V. Detailed

dx.doi.org/10.1021/cr3000626 | *Chem. Rev.* XXXX, XXX, XXX−XXX

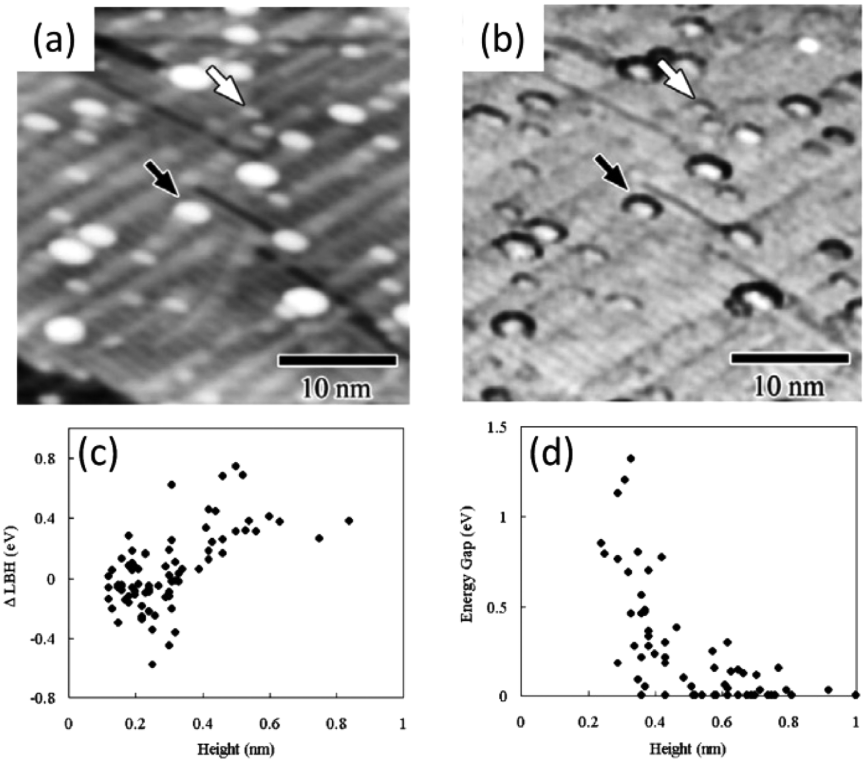

Figure 23. (a) STM and (b) LBH images of the Au-deposited TiO_2(110)-(1 × 2) surface. The white and black arrows indicate Au particles. Size dependence of (c) the relative LBH and (d) the energy gap of the Au particles on the TiO_2(110)-(1 × 2) surface. The ΔLBH was defined as the LBH difference between the particle (LBH_{Au}) and the substrate (LBH_{TiO_2}): $\Delta LBH = LBH_{Au} - LBH_{TiO_2}$. Reprinted with permission from ref 119. Copyright 2004 Elsevier.

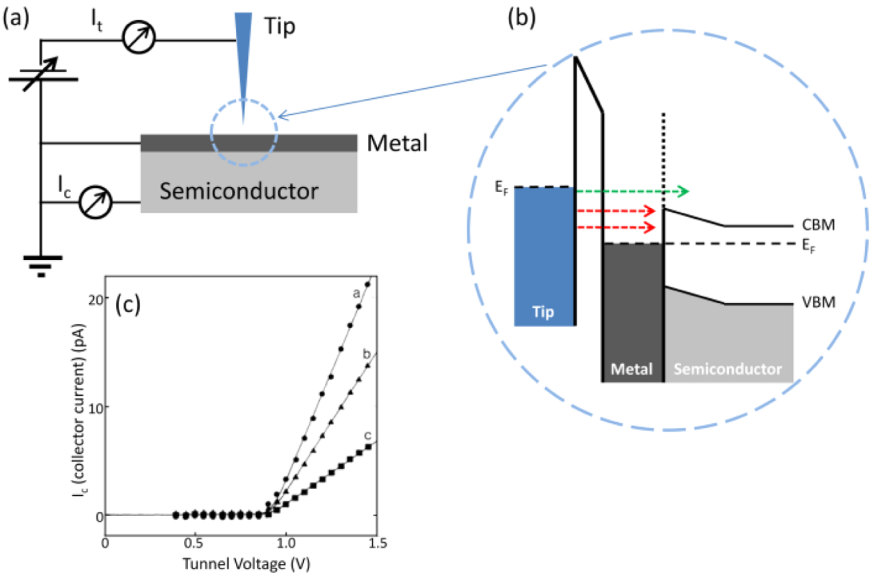

Figure 24. (a) Schematic diagram and (b) energy-band diagram of the three-terminal BEEM experiment. (c) BEEM spectroscopy results for the Au−Si heterojunction. BEEM spectra of collector current I_c vs tunnel voltage V are shown. Spectra a (●), b (▲), and c (■) were measured at tunnel currents of 0.87, 0.57, and 0.27 nA, respectively. Adapted with permission from ref 121. Copyright 1988 the American Physical Society.

discussion and application of BEEM imaging and spectroscopy can be found in refs 124−126.

2.5. O_2 Photostimulated Desorption (PSD) and Electron-Stimulated Desorption (ESD)

All the methods that we discussed so far use the physical properties of a semiconductor (such as electronic structure, photoluminescence, surface potential, etc.) for measuring band bending. Photochemical reactions on the surface can provide another way to measure band bending.

Previous PL and SPV discussions indicate that the presence of near-surface electric field associated with band bending can separate the electron−hole pair and repel the hot electron and hole in different directions. As shown in Figure 17, upward band bending will repel the electrons toward the bulk and

dx.doi.org/10.1021/cr3000626 | Chem. Rev. XXXX, XXX, XXX−XXX

attract the holes toward the surface, which will cause surface hole enrichment. Meanwhile, the presence of an electric field will also change the tunneling probability of electrons and holes between the semiconductor surfaces and adsorbed molecules. As shown in Figure 25a, the upward bent bands increase the barrier width and height for electron tunneling from the CB of the semiconductor to an unfilled orbital of an adsorbed molecule, decreasing the electron transmission probability from the semiconductor to the adsorbate. On a surface with downward bent bands (Figure 25b), the tunneling barrier is eliminated, which facilitates the electron transfer across the surface to the molecule. For hole transport, the effect is reversed. Overall, upward band bending will *depress* the availability of hot *electrons* from semiconductor to adsorbate, while *increasing* the availability of *holes* from semiconductor to adsorbate.

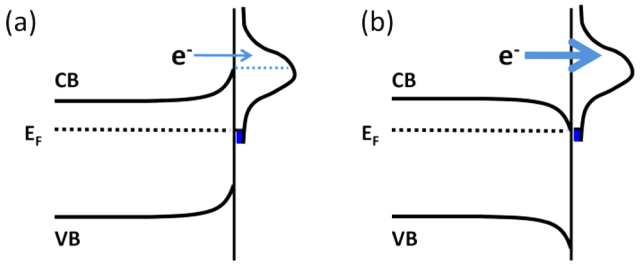

Figure 25. Effects of (a) upward band bending and (b) downward band bending on the tunneling probability of hot photogenerated electrons from a semiconductor to an adsorbed molecule.

The excited electrons and holes in the semiconductor will cause different photoreactions on the surface.[6,7,11] One of the well-known experiments is the O_2 ESD/PSD experiment. Previous experiments[7,127−132] and DFT calculations[133] showed that O_2 desorption is caused by excited holes in the TiO_2, which are produced by incident electrons or photons. The hole-mediated desorption of adsorbed O_2 can be described by

$$h + O_2^- \xrightarrow{k} O_2(g)\uparrow \quad (18)$$

Then, the O_2 desorption rate is $-d[O_2^-(a)]/dt = k[O_2^-(a)] \times [h]$, where $O_2^-(a)$ is the adsorbed O_2 coverage and $[h]$ is the surface hole concentration produced at steady state during illumination. The variation of the hole concentration produced by UV light can be quantitatively measured by monitoring the O_2 desorption rate caused by incident electrons or photons. The effect of band bending by an adsorbate molecule can then be measured by observing the rate of O_2 desorption.

Figure 26 shows a schematic diagram of the equipment for measuring the PSD/ESD of O_2 on a $TiO_2(110)$ surface.[128,134] A clean $TiO_2(110)$ surface with 8−10% bridge-bonded oxygen vacancies can be prepared by Ar^+ sputtering followed by annealing at 900 K in UHV. Previous experiments indicated that chemisorbed O_2 was detected on UHV-annealed $TiO_2(110)$ after exposure of O_2 at low temperature (~100 K). The preadsorbed O_2 can be desorbed by electrons or photons with incident energy higher than the TiO_2 bandgap.[127−129,134] Desorbing O_2 can be detected by a line-of-sight quadrupole mass spectrometer (QMS). A typical QMS measurement of the ESD of $^{18}O_2$ on the $TiO_2(110)$ surface is shown in the right section of Figure 26 with 100 eV incident electrons. The $^{18}O_2$ QMS signal quickly reaches the maximum value after the electron current is on (within the time resolution of 0.2 s). Then it decreases monotonically with time due to desorption and dissociation of O_2 on $TiO_2(110)$ by the incident electrons.[30,78,132,134] The O_2 PSD curve is similar to this ESD curve.[6,7,127−129] In our ESD/PSD measurements, the initial rate of O_2 desorption by ESD/PSD (dashed circle in right part of Figure 26) was chosen for measurement to avoid damage effects caused by the incident electrons and photons. The O_2-QMS signal is directly proportional to the rate of O_2 desorption ($-d[O_2(a)]/dt$).

The detailed experiment using ESD/PSD for measuring band bending will be discussed in section 3. It is shown that O_2 desorption may be used to monitor the rate of hole transfer to adsorbed O_2, giving a very useful method to observe excitation and transport for photoexcited holes.

2.6. Other Measurement Methods

Besides the above-mentioned methods, there are several other methods that can measure the band bending, such as Raman

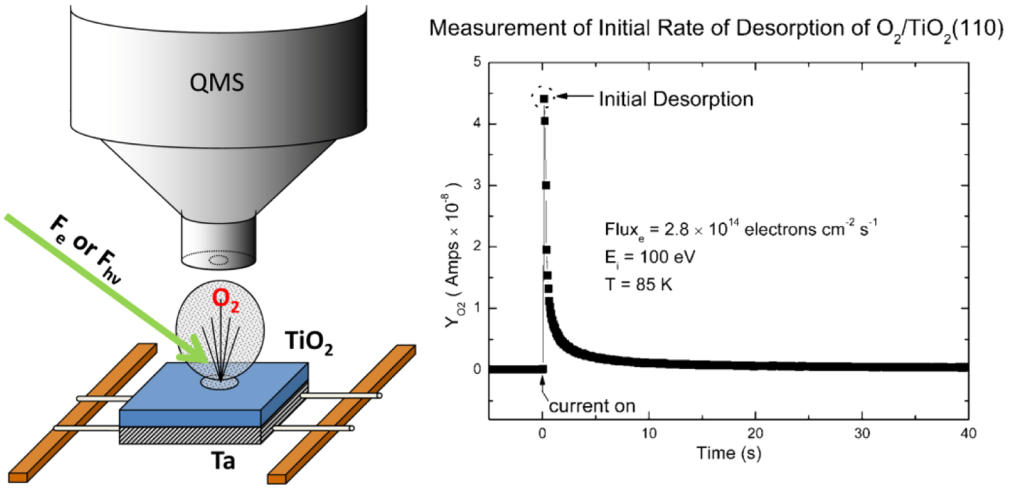

Figure 26. (left) Schematic diagram for the experimental apparatus used to measure PSD or ESD of O_2 from $TiO_2(110)$ and (right) electron-stimulated desorption measurements for $^{18}O_2$ on the $TiO_2(110)$ surface using a QMS. $^{18}O_2$ is adsorbed to saturation coverage at 85 K onto vacancy defects in the surface. Adapted with permission from refs 128 and 134. Copyright 2005 and 2010 American Chemical Society.

dx.doi.org/10.1021/cr3000626 | *Chem. Rev.* XXXX, XXX, XXX−XXX

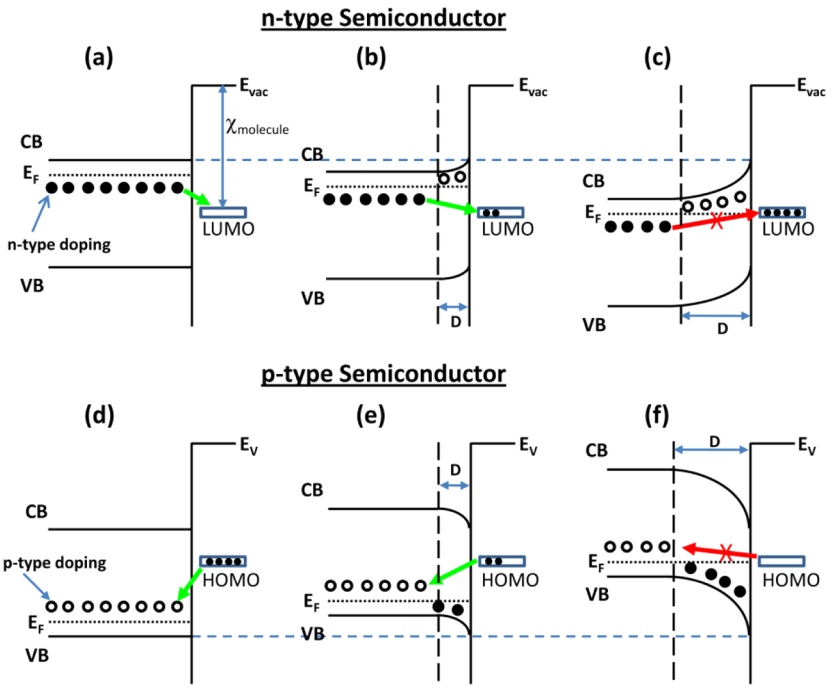

Figure 27. Energy diagram of (a–c) n-type and (d–f) p-type semiconductors (a, d) before, (b, e) after partial, and (c, f) after equilibrium chemisorption on the surface. Adapted with permission from ref 149. Copyright 1953 American Institute of Physics. For the n-type semiconductor, the dark circles represent excess electrons characteristic of n-type doping. The open circles represent holes produced by transfer of electrons to the LUMO or in the case of p-doped semiconductor the holes left by charge transfer between atoms in the semiconductor itself. The outward charge transfer produced a Helmholtz layer of negative charge causing upward band bending. For the p-type semiconductor, electrons from a HOMO orbital transfer to the substrate and the net surface charge became positive, causing downward band bending. *D* is the thickness of the depletion or accumulation layer for two cases.

scattering,[135] high-resolution electron energy loss spectroscopy (HREELS),[136–138] current–voltage (*I–V*),[14,139,140] capacitance–voltage (*C–V*),[13,140] electron-beam induced voltage (EBIV),[141–143] electron-beam induced current (EBIC),[140,141,144] and photocurrent measurements.[145–147]

3. EFFECTS OF BAND BENDING ON PHOTOCHEMISTRY PROCESSES

An overview of band bending effects on thermally activated adsorption on semiconductor surfaces and on charge transfer at the molecule/semiconductor interface is given in section 3.1. The detailed factors influencing band bending and photochemistry in photocatalytic systems will be discussed in sections 3.2–3.7. In the last section (section 3.8), the applications of band bending and the role of electrons and holes on different photocatalytic systems will be discussed.

3.1. Overview of Band Bending Effects on Photochemistry

There are three important elementary processes on a solid catalyst surface during heterogeneous photocatalytic processes: (1) the adsorption of reactive molecules; (2) the photoactivated reaction between adsorbed molecules mediated by the substrate; (3) the desorption of product molecules.[148] Consequently, band bending may influence the photochemistry processes on a semiconductor in the following ways: (1) band bending can influence the thermal adsorption or desorption of reactant or product molecules on the semiconductor substrate; (2) band bending can influence the photoreaction process by modulating photoexcited charge carrier recombination and transfer processes between the semiconductor and adsorbate.

3.1.1. Band Bending and Molecular Adsorption or Desorption. Figure 27 shows the influence of band bending on the chemisorption of gas molecules on semiconductor surfaces.[149] Figures 27a–c show the adsorption of an electron acceptor molecule on an n-type semiconductor. When a molecule approaches an n-type semiconductor surface, the electrons associated with n-type dopants will transfer to the lowest unoccupied molecular orbital (LUMO) of the molecule forming a negative charge layer at the semiconductor surface. This can occur only if the LUMO energy is lower than the Fermi level. Meanwhile, the development of upward band bending reduces the energy difference between the Fermi level and LUMO orbital. (The vacuum level, E_{vac}, is chosen as the 0 reference for considering the molecule–surface interaction.[150]) After adsorbing more molecules, the Fermi level, which bears a constant relationship to the bottom of the bulk conduction band, decreases to the same energy as that of the LUMO level (Figure 27c). Then the electrons of the semiconductor cannot transfer to the LUMO level any more, and the coverage of the adsorbed acceptor molecule reaches saturation. Similarly, on a p-type semiconductor surface (Figures 27d–f), if the electron potential energy of the highest occupied molecular orbital (HOMO) of the adsorbed molecule is higher than the empty states in the semiconductor, then electrons will transfer from the adsorbed molecules (electron donor) to the p-type semiconductor causing downward band bending. Taking the vacuum level, E_{vac}, as a reference, the presence of downward band bending on the semiconductor surface raises the Fermi level and the doping levels, but the energy of the HOMO orbital remains unchanged. The saturation adsorbate coverage is attained when the Fermi level reaches the HOMO level of the adsorbed molecule (Figure 27f).

dx.doi.org/10.1021/cr3000626 | *Chem. Rev.* XXXX, XXX, XXX–XXX

The above model qualitatively indicates that the saturation adsorption coverage of donor and acceptor molecules on semiconductor surfaces will be influenced by band bending. In addition adsorption is influenced by the effects of active defect site availability and adsorbate−adsorbate interactions on a semiconductor surface.[149−154] It is known that the band bending (V_{BB}) potential can be calculated from eq 9, $V_{BB} = (eN_dD^2)/(2\varepsilon_r\varepsilon_0)$, where e is the electronic charge, N_d is the n-type dopant density, D is the depletion layer thickness, ε_r is the relative permittivity of the semiconductor, and ε_0 is the permittivity of vacuum. From Figure 27a−c, the band bending and depletion layer are caused by the adsorption of molecules on the surface. If we assume $N_dD = N_s$ (i.e., the charge of the n-type dopant in the depletion layer has been transferred to the adsorbed molecules), then

$$V_{BB} = \frac{eN_dD^2}{2\varepsilon_r\varepsilon_0} = \frac{eN_s^2}{2N_d\varepsilon_r\varepsilon_0} \quad (19)$$

From Figure 27a−c, the maximum amount of band bending is equal to the potential difference between the unfilled LUMO and the Fermi level. In an n-type semiconductor, V_{BB} equals $(\chi_{molecule} - \phi)$, where $\chi_{molecule}$ and ϕ are the electron affinity of the molecule and the work function of the surface, respectively. Then the maximum concentration of adsorbed molecules on the surface ($N_{s,max}$) is

$$N_{s,max} = \left(\frac{2N_d\varepsilon_r\varepsilon_0V_{BB}}{e}\right)^{1/2} = \left[\frac{2N_d\varepsilon_r\varepsilon_0(\chi_{molecule} - \phi)}{e}\right]^{1/2} \quad (20)$$

This equation quantitatively indicates that the limitation of band bending will limit the coverage of adsorbed molecules. Thus for TiO_2, with $\varepsilon_r \approx 100$, if we assume $V_{BB} = 1$ V and $N_d = 10^{20}-10^{25}$ m^{-3}, $N_{s,max} = 7 \times 10^{14}$ to 2.3×10^{17} m^{-2}, which is about 10^{-4} ML to 5×10^{-2} ML.

3.1.2. Band Bending and Photoexcited Charge Carrier Transfer and Recombination. There are two kinds of initial photoexcitation processes on a heterogeneous photocatalyst surface:[6] (1) direct photochemical excitation where the initial photoexcitation process occurs in an adsorbed molecule; (2) indirect photochemical excitation where the initial photoexcitation process occurs in the semiconductor substrate followed by charge transfer from the substrate to adsorbed molecules. In this section, the influence of band bending on the two initial photoexcitation processes will be discussed.

3.1.2.1. Band Bending and Direct Photochemical Excitation. During the surface sensitization of the photochemistry process, the influence of band bending on the charge and energy transfer between excited dye molecules and semiconductor surfaces may be employed to influence the charge collection or photoreaction efficiency. A detailed discussion can be found in several reviews.[15,155,156] Figure 28 gives simplified schematic diagrams of the electron transfer processes at the interface between an n-type semiconductor and a dye molecule during a direct photochemical excitation process. In an n-type semiconductor with upward band bending (Figure 28a), the excited electron from the LUMO of an adsorbed dye molecule (light absorber) can be injected into the semiconductor and transferred away from the interface and into the bulk (indicated by the green arrows). This process occurs because of the electric field from the surface to the bulk. However, in the semiconductor with downward band bending (Figure 28b), the injected electrons from the excited dye molecule cannot go deep into the bulk and will accumulate at the surface due to the presence of an opposite electric field from the surface to the bulk. Finally, the electron may jump back into the HOMO of the adsorbed dye molecule causing surface quenching of the excitation process (indicated by the blue arrow in Figure 28b). It is also found for upward band bending that the surface quenching occurs by tunneling of the injected electrons through the space charge layer (indicated by the blue arrow in Figure 28a). By tuning the dopant density in the semiconductor, the influence of the thickness of the space charge layer on the surface quenching and charge transfer has been investigated by several groups.[155,157−159]

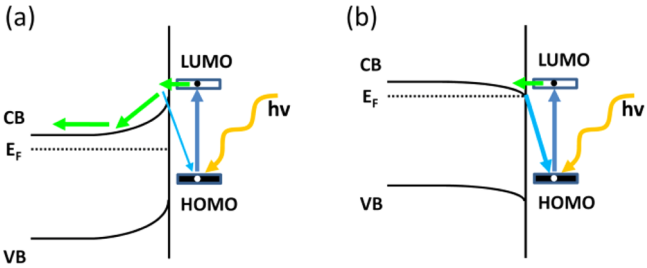

Figure 28. The influence of band bending on the electron transfer and surface quenching of a dye molecule at a molecule/semiconductor interface: (a) upward band bending; (b) downward band bending.

3.1.2.2. Band Bending and Indirect Photochemical Excitation. Figure 29 schematically shows the excitation and deexcitation processes in a colloidal semiconductor.[6] The electron in the VB can be excited to the CB by the absorption of a photon with energy higher than the bandgap leaving a hole in the VB. This occurs via the production of an exciton (*) which evolves into a separated electron−hole pair. The deexcitation of the produced electron−hole pair may occur by two processes: (1) the hot electron and hole may recombine on the surface (process A) or in the bulk (process B) of the semiconductor; (2) the hot electron and hole may migrate to the surface and react with the adsorbed surface species causing oxidation and reduction surface photoreactions (processes C and D).

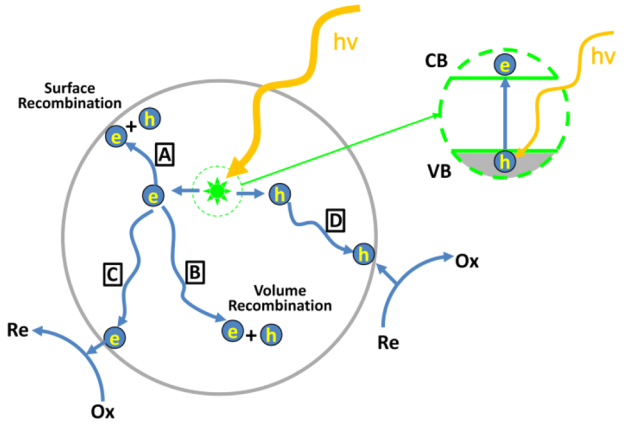

Figure 29. Schematic of photoexcitation in a solid particles followed by deexcitation events. Reprinted with permission from ref 6. Copyright 1995 American Chemical Society.

Usually, the efficiency of photoreaction is expressed by the quantum yield (Φ), which is

dx.doi.org/10.1021/cr3000626 | Chem. Rev. XXXX, XXX, XXX−XXX

$$\Phi = \frac{\text{rate of reactant consumption or product formation}}{\text{rate of photon absorption}} \quad (21)$$

From the above discussion of Figure 29, the rate of reactant consumption or product formation is proportional to the rate of charge (electron/hole) transfer (k_{CT}) from the semiconductor to the reactant molecules, and the rate of photon absorption is proportional to the sum of the rates of the charge transfer (k_{CT}) and electron−hole recombination (k_R). In other words, Φ can be expressed as[6]

$$\Phi \propto \frac{k_{CT}}{k_{CT} + k_R} \quad (22)$$

Obviously, the band bending effect will influence the rate of electron/hole transfer and recombination thus influencing the efficiency of the photoreaction. In the discussion of section 2.2, the PL spectral intensity gives clear evidence that upward/downward band bending causes changes in the near-surface electric field. This facilitates the spatial separation of hot electron−hole pairs and depresses the recombination rate (k_R). On the other hand, the direction of band bending will also influence the electron/hole availability for charge transfer to the surface. For upward band bending, the direction of the electric field (from the bulk to the surface) will increase the hole availability at the surface thus increasing a hole-induced surface reaction. For downward band bending, the direction of the electric field (from the surface to the bulk) will increase the hot electron availability at the surface thus increasing an electron-induced surface reaction. The following sections will give detailed examples about the effects of band bending on photochemistry processes.

3.2. Particle Size-Induced Band Bending and Photochemistry

Semiconductor nanoparticles are extensively used to induce photochemistry processes.[160,161] Three differences exist between nanoparticle semiconductors and planar semiconductors: (1) differences in the magnitude of band bending, (2) possible quantum size effects, and (3) increased surface-to-volume ratio. Using the Poisson−Boltzmann equation, the potential distribution in a spherical semiconductor particle with radius r_0 has been developed by Albery and Bartlett.[162] In an n-type semiconductor nanoparticle, the band bending (V_{BB}), that is, potential difference, at distance r with reference to the center of the particle is

$$V_{BB}(r) = \frac{kT}{6e}\left[\frac{r - (r_0 - D)}{L_D}\right]^2\left[1 + \frac{2(r_0 - D)}{r}\right] \quad (23)$$

where L_D is the Debye length [$L_D = (\varepsilon_r\varepsilon_0 kT/e^2N_d)^{1/2}$], D is the depletion length, and r_0 is the radius of the semiconductor nanoparticle. As shown in Figure 30, for large particles ($r_0 \gg D$), the band bending from surface to the center is

$$V_{BB}(r_0) = \frac{kT}{2e}\left(\frac{D}{L_D}\right)^2 = \frac{eN_dD^2}{2\varepsilon_r\varepsilon_0} \quad (24)$$

which is the same as for the planar sample as we discussed in eq 9. (The planar sample can be treated as a particle with infinite diameter.) For a small particle with $r_0 < \sqrt{3}D$, the band bending from surface to the center is

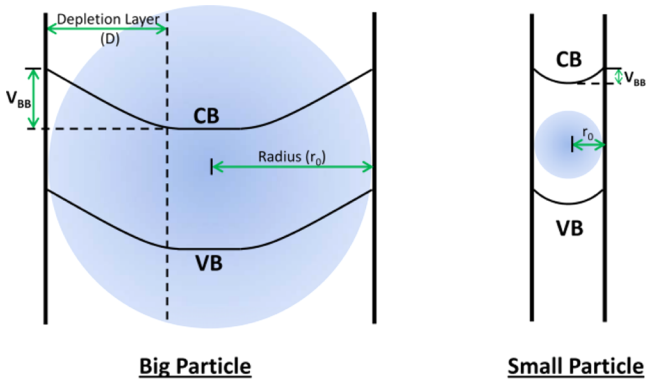

Figure 30. Schematic diagrams of the band bending in big and small particles. Adapted with permission form ref 160. Copyright 1995 American Chemical Society.

$$V_{BB}(r_0) = \frac{kT}{6e}\left(\frac{r_0}{L_D}\right)^2 = \frac{er_0^2N_d}{6\varepsilon_r\varepsilon_0} \quad (25)$$

Equation 25 indicates that there are three variables, particle size (r_0), dopant concentration (N_d), and relative dielectric constant (ε_r), determining the magnitude of band bending in small particles:

(1) Particle size. The band bending will decrease with the size of the semiconductor particle. When the particle radius equals L_D (for TiO_2, L_D is ∼3.8−12 nm with $\varepsilon_r \approx 100$,[76,163] $N_d \approx 10^{24}$−10^{25} m^{-3}[164]), the band bending from the particle center to surface is only ∼0.004 V at room temperature. It is reported that the absence of band bending in small nanoparticles significantly enhances the sensitivity of gas sensors composed of the nanoparticles.[165,166] On the other hand, the lack of band bending may depress the photoactivity in such particles. Ohno et al.[161,167,168] found that photocatalytic oxidation of water can take place on large rutile TiO_2 particles while not on small anatase particles in the presence of Fe(III) ions in solution. Based on the previous experimental results that upward band bending is required for the photooxidation of water on a TiO_2 electrode surface,[169,170] the authors reasoned that the high photoactivity is due to the presence of upward band bending in larger particles.

(2) Dopant concentration. The band bending in the nanoparticle may be enhanced by increasing the dopant concentration.[171−174] For example, enhanced photocatalytic activity of rare-earth-doped TiO_2 nanoparticles has been found in the photodegradation of the nitrite ion.[173] Further studies indicate that there exists an optimal concentration of rare earth metal doping at ∼0.5 wt % for this system. A schematic explanation is shown in Figure 31. The upper parts are the energy band diagrams, and the lower parts are the schematic diagrams of the photogenerated electron and hole behavior in the particles. When the dopant concentration is low (Figure 31a), the band bending value is negligible and the excited electron/hole pair in the photon penetration region (yellow part) cannot be separated effectively due to the flat energy band. Most of the excited electrons and holes will recombine in the bulk or in the surface region, and therefore the photocatalytic efficiency is low. As we increase the dopant concentration, the band bending

dx.doi.org/10.1021/cr3000626 | Chem. Rev. XXXX, XXX, XXX−XXX

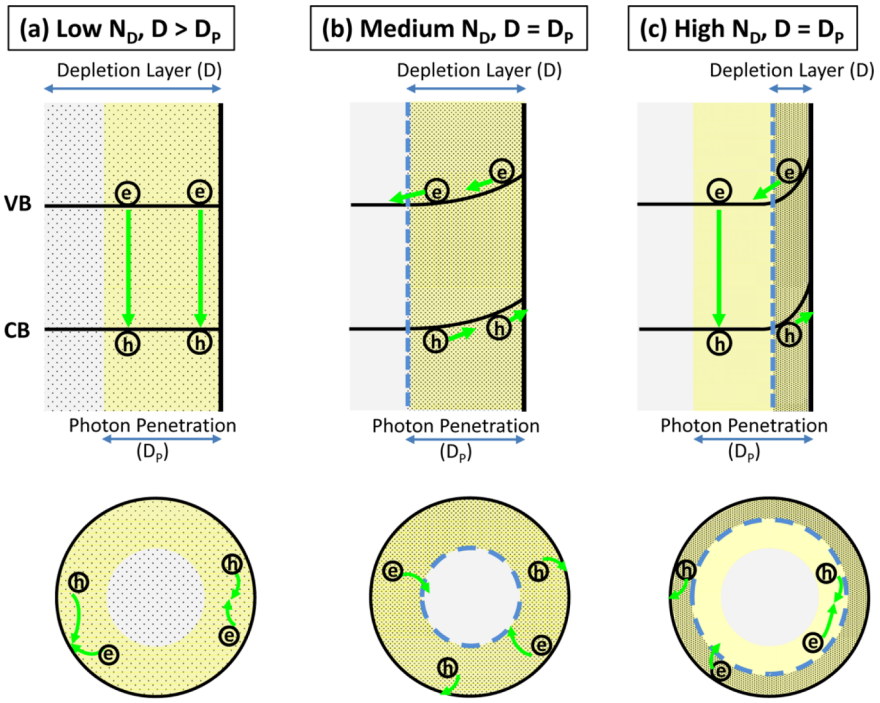

Figure 31. The effect of dopant concentration (N_D) on the band bending and photogenerated carrier behavior in semiconductor nanoparticles: (a) The dopant concentration is low; depletion layer length (D) > photon penentration (D_P); (b) the dopant concentration is medium; depletion layer length (D) = photon penentration (D_P); (c) the dopant concentration is high; depletion layer length (D) < photon penetration (D_P). In panel c, where extreme upward band bending exists because of high N_D, holes are efficiently transferred to the particle surface.

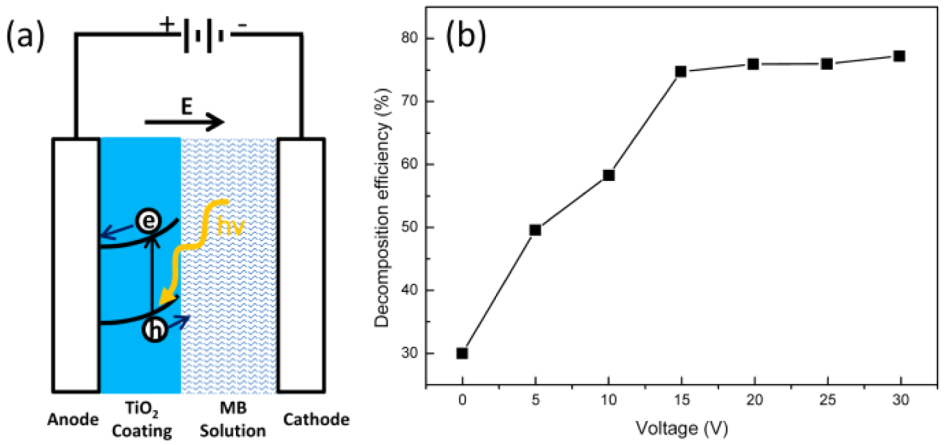

Figure 32. (a) Schematic diagram of the equipment for the investigation of the photodegradation of methylene blue (MB) in the presence of an externally applied electric field. (b) Voltage dependence of the photodecomposition efficiency of methylene blue on a TiO_2 coating of 11 μm thickness. Adapted with permission from ref 181. Copyright 2008 Elsevier.

inside the particles will also increase. Meanwhile, the depletion layer or space charge region (shadowed part) will also decrease in depth. When the depletion layer becomes equal in depth to the photon penetration depth (Figure 31b), the photogenerated electron−hole pair can be separated with maximum efficiency leading to lowered recombination rate, and the photocatalytic efficiency reaches its highest value. As the dopant concentration increases still further, the depletion region decreases in depth to become less than the photon penetration region, and only the photogenerated electron−hole pair in the depletion region can be separated effectively (Figure 31c). Consequently, a further increase of dopant concentration will decrease the photocatalytic efficiency. (It should be noted that sometimes the dopant can also act as a recombination site, which may also decrease the photocatalytic efficiency.[175])

(3) Dielectric constant. The relationship between the dielectric constant and photochemistry has been barely discussed so far. The charge transport and carrier lifetime in dye-sensitized solar ZnO and TiO_2 solar cells, which are made with approximately equal size ZnO and TiO_2 nanoparticles, have been studied by Quintana et al.[176] It was found that the photogenerated electron lifetime is significantly higher in ZnO than in TiO_2, which may due to the significant band bending in ZnO particles resulting in larger energy barriers for electron transport and increased band bending leading to decreased recombi-

dx.doi.org/10.1021/cr3000626 | Chem. Rev. XXXX, XXX, XXX−XXX

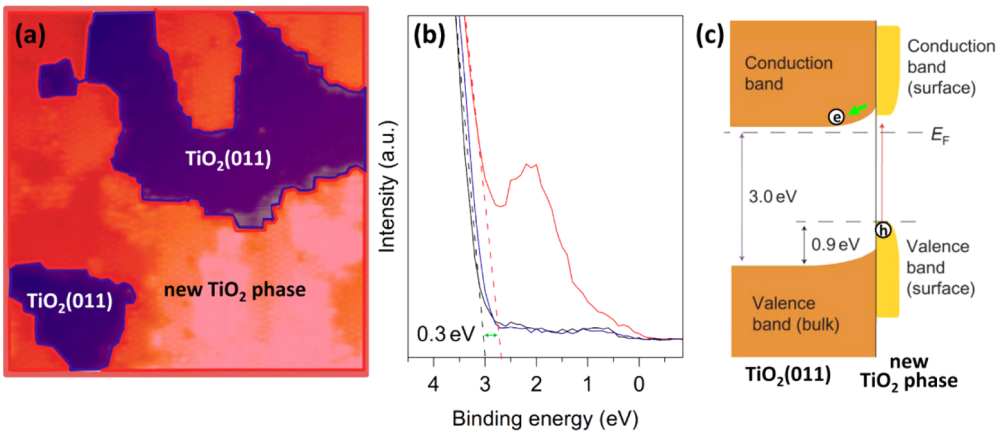

Figure 33. (a) STM image of rutile $TiO_2(011)$ surface showing the coexistence of the original $TiO_2(011)$-2 × 1 surface (blue region) and a new TiO_2 phase (red region). (b) UPS spectra of original $TiO_2(011)$-2 × 1 surface (black and blue curves) and $TiO_2(011)$ surface after low-pressure oxidation and partial formation of the new TiO_2 phase (red curve). (c) Band diagram of the new TiO_2 phase/$TiO_2(011)$, deduced from UPS and STS, together with an indication of the bandgap contraction within the new TiO_2 phase leading to the 2.2 eV feature in the UPS spectrum. Adapted with permission from ref 189. Copyright 2011 Macmillan Publishers Ltd. [Nature Chemistry].

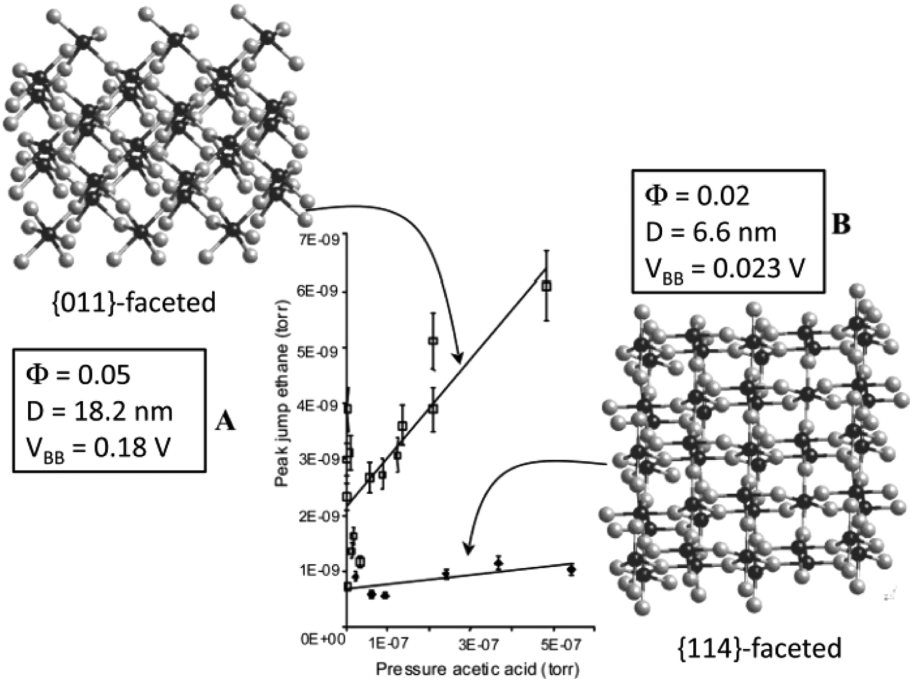

Figure 34. The two stable reconstructured surfaces of a $TiO_2(001)$ single crystal. Black balls, Ti atoms; gray balls, O atoms. The plot (center) shows the formation of the main reaction product (ethane) as a function of acetic acid pressure under steady-state conditions in ultrahigh vacuum based on mass spectroscopy. Also shown are the estimated width of the depletion layer (D) and barrier height (V_{BB}) from the experimental quantum yield (Φ) of the reaction of acetic acid on both surfaces. Reprinted with permission from ref 191. Copyright 2002 American Chemical Society.

nation. The band bending in a TiO_2 particle ($\varepsilon \approx 50-100$) would be much less than that in the ZnO particle as a result of the lower ZnO dielectric constant ($\varepsilon \approx 8$)[177] assuming the same dopant concentration.

3.3. External Electric Field Induced Band Bending and Photochemistry

The effect of an external electric field on thermally activated chemisorption and catalysis has been studied before.[178−180] Herein, we mainly discuss the effect of electric field induced band bending on the photochemistry process. The physical principle of external electric field induced band bending has been discussed in section 1.1. Taking the photodegradation of methylene blue (MB) dye solution as an example, Figure 32a shows a schematic diagram of the equipment.[181,182] A thermal-sprayed TiO_2 film on the anode was used as the photocatalyst. The efficiency of photodecomposition of methylene blue increases with increasing bias voltage (Figure 32b). The maximum efficiency reaches ~80%, which is more than two times the efficiency observed without an applied external voltage ($V = 0$). It is believed that methylene blue decomposition is catalyzed by the excited holes. The presence of an electric field from the anode to cathode causes upward band bending near the interface between the TiO_2 film and the methylene blue solution, which depresses the electron−hole recombination rate and increases the hole availability at the TiO_2/solution interface. The increased hole availability

dx.doi.org/10.1021/cr3000626 | Chem. Rev. XXXX, XXX, XXX−XXX

increases the photodecomposition efficiency of methylene blue. It is also found that the combination of Ag deposition with the application of an external electric field can significantly enhance the rate of photocatalytic oxidation of formic acid on the TiO_2 film.[183]

3.4. Surface Structure-Induced Band Bending and Photochemistry

Surface structure can influence photocatalytic performance either by tuning the adsorption of reactants (thermal surface sensitive processes)[184] or by tuning the charge carrier behavior (photochemistry/physics process). Herein, we focus on the surface structure-induced band bending and related photochemistry. The surface structure is determined either by the natural surface reconstruction of a single crystal or by the selection of a specific crystallographic surface orientation that does not reconstruct.

3.4.1. Surface Reconstruction. Surface reconstruction on a semiconductor surface can induce band bending. It is known that Ti interstitial species in the TiO_2 bulk can diffuse to the surface in the presence of oxygen and form a new TiO_2 phase on the surface.[44,45,185−189] As an example, Figure 33a shows a new TiO_2 phase (red region) formed on the surface of the rutile TiO_2(011) surface (blue region) after annealing in a 1×10^{-6} Torr O_2 atmosphere.[189] STM and STS studies indicated that the new TiO_2 phase presents a different atomic arrangement and electronic structure from the original rutile TiO_2(011) surface. UPS spectra (Figure 33b) showed that the presence of the new TiO_2 phase bends the bulk bands upward by ∼0.3 eV. A band diagram is shown in Figure 33c. Band bending, as shown, promotes hole transport to the surface upon UV irradiation.

The effect of surface reconstruction of a TiO_2(001) single crystal on the photoreaction of acetic acid has been studied by Wilson and Idriss.[190,191] Annealing TiO_2(001) in vacuum at 700−750 and 900−950 K can produce {011}- and {114}-faceted reconstructed surfaces, respectively. For the photocatalytic reaction of acetic acid, the quantum yield of the low-temperature annealed surface ({011}-facet surface) is 2.5 times that of high-temperature annealed surface ({114}-facet surface). The depletion layer length (D) can be calculated by the measured quantum yield (Φ),[190−192]

$$D = \frac{\Phi}{\alpha} + L(\Phi - 1) \tag{26}$$

where α is the reciprocal absorption length, and L is the minority carrier diffusion length. The band bending value (V_{BB}) can also be obtained by eq 9. The calculated values of the depletion layer length and band bending are indicated in Figure 34. The higher photocatalytic reactivity of the {011}-facet surface is due to the low electron−hole recombination rate caused by the broad depletion layer and high upward band bending. This example gives clear evidence that a change of the outer layer structure of a semiconductor can change the photocatalytic activity significantly.

3.4.2. Crystallographic Surface Orientation. Although many experimental results[193−198] indicate that the photocatalytic performance of semiconductors is surface-dependent, the detailed mechanism is still ambiguous. Band bending may also play a role among the numerous factors, such as surface atomic structure and related chemisorptions,[198−201] anisotropic band dispersion,[202] dipolar field effect,[203−209] and surface energy levels.[194] Several effects of surface orientation on band bending and photocatalysis are discussed below.

(1) The Effect of Surface Work Function and Dielectric Constant. In solution, the band bending near the semiconductor surface is determined by the surface work function and solution redox potential.[150] Different surface orientations will influence the surface work function and hence the near surface band bending in a semiconductor. Furthermore, the anisotropic dielectric constant may also contribute to the surface-dependent photocatalytic efficiency. Taking rutile TiO_2 as an example, it is reported that the dielectric constants parallel to the [001] and the [100] direction are 170 and 86, respectively.[201,210] According to the space charge layer thickness equation (eq 10), the space charge region at the (001) surface (along [001]) is ∼1.4 times the length at the (100) surface (along [100]). Assuming the space charge region is smaller than the photon absorption length, the longer space charge region will prohibit electron−hole recombination (similar to Figure 31b,c) and hence increase the photocatalytic efficiency.

(2) The Effect of Surface Atomic Structure Induced Chemisorption. The surface chemistry on different surface orientations due to different surface atomic structure may also induce different degrees of band bending. Photocatalytic degradation of methyl orange dye over single crystalline ZnO has been investigated, showing that the positive Zn-terminated ZnO surface (ZnO(0001)-Zn) had more photocatalytic activity than the negative O-terminated ZnO surface (ZnO(0001)-O).[199] The difference in chemisorption-induced band bending in the solution has been employed by the authors to explain the different activity of the two surfaces. On the positive ZnO(0001)-Zn surface, the surface is terminated by OH^- species in solution, which induces upward band bending enhancing the hole-mediated photocatalytic process. Conversely, the negative ZnO(0001)-O surface is terminated by H^+ species in solution, which induces downward band bending, decreasing the hole-mediated process.

(3) The Effect of Dipolar Field in a Ferroelectric Crystal. The spontaneous polarization in the domains of ferroelectric materials can bend the energy bands and separate photogenerated electron and holes effectively.[211−213] Spatially localized photochemical reactions have been found on the surfaces of ferroelectric crystals.[203−209] The reactive facets can be identified by the formation of insoluble reaction products on the corresponding surfaces. For example, Figure 35a,b gives the SEM images of the photoreduction of Ag^+ ($Ag^+ + e = Ag^0$) on $BaTiO_3$ microcrystals.[203] The deposited Ag can be identified by the white particles on the (100) and (111) surfaces in Figure 35b. The relative reactivity of the surfaces follows the order {100} > {111} > {110}. The surface-dependent reactivity is related to the dipolar field in the ferroelectric crystal. A simplified diagram showing charge transfer and band bending at different $BaTiO_3$ facets is indicated in Figure 35c. An internal polarization (left direction in this case) due to the pinning of ferroelectric domains in a preferred orientation will force photogenerated electrons/holes to the right/left, bending the energy band upward/down-

dx.doi.org/10.1021/cr3000626 | Chem. Rev. XXXX, XXX, XXX−XXX

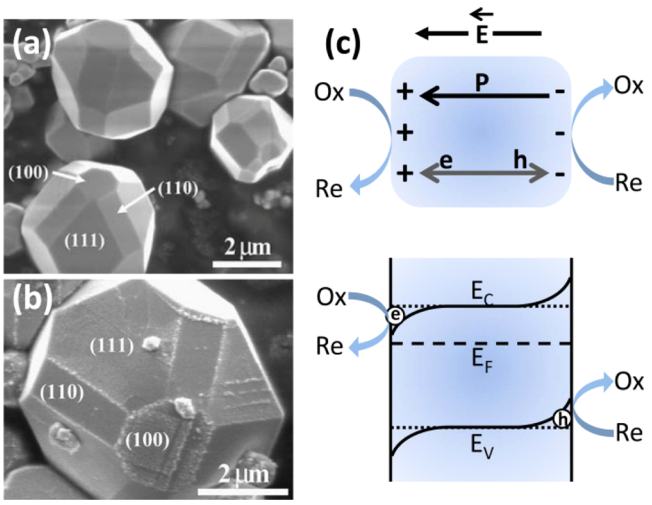

Figure 35. SEM images of faceted $BaTiO_3$ crystals (a) before and (b) after photoreaction in aqueous $AgNO_3$ solution. The crystallographic orientations of the faces are labeled. The bright particles in panel b correspond to silver deposits. (c) The polarization, *P*, forces the photogenerated electrons and holes to opposite sides in the particle. This results in the reduction and oxidation reactions on different sides of the particles. Adapted with permission from ref 203. Copyright 2008 Springer.

ward in the right/left. This results in oxidation/reduction reactions on the right/left sides of the particles. It is found that even the surfaces with the same orientation but different polarization direction have different photochemical behavior.[208]

3.5. Gas-Adsorption-Induced Band Bending and Photochemistry

Molecules can be generally divided into two categories, electron donor or acceptor molecules, which are designated on the basis of the electron transfer direction from the molecule to the semiconductor or from the semiconductor to the molecule. On the TiO_2 surface, CH_3OH[214,215] and NH_3[99,216] are electron donor molecules, and O_2[44,76,217,218] and Cl_2[219] are electron acceptor molecules. A schematic diagram of the influence of adsorbed electron acceptor and donor molecules at a semiconductor surface on the band bending and photocatalytic behavior is provided in Figure 36. The adsorption of acceptor molecules on the semiconductor surface will bend the energy bands upward. The produced electric field near the semiconductor surface will separate the electron–hole pair reducing the rate of recombination and promoting hole transport to the surface. Conversely, the adsorption of donor molecules on the semiconductor surface will bend the energy bands downward. The produced electric field near the semiconductor surface then separates the electron–hole pairs and promotes the electron transport to the donor-modified surface.

Most photochemistry experiments are carried out in solution on semiconductor particles, which may integrate the effects of particle size, surface morphology, impurity, and solution-related chemistry. Working on single crystals in ultrahigh vacuum and with surfaces which are atomically clean removes many of these uncertainties. Studies of PSD (photon stimulated desorption) and ESD (electron stimulated desorption) of O_2 on the $TiO_2(110)$ single crystal surface therefore offers a simple and clean way of understanding band bending and related photochemistry. Here both photons and incident electrons

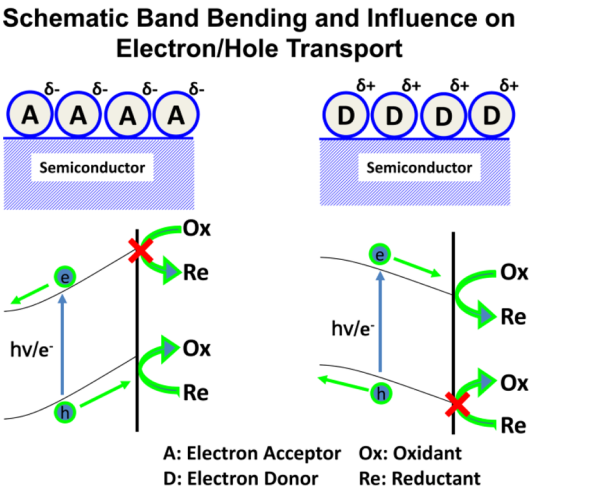

Figure 36. Schematic diagram of band bending and its effects on hole or electron transport causing oxidation or reduction reaction by adsorption of electron acceptor or donor molecules. Reprinted with permission from ref 30. Copyright 2010 American Chemical Society.

are envisioned as producing electron–hole pairs in the $TiO_2(110)$.

The effects of Cl_2 (electron acceptor) and CH_3OH (electron donor) on the ESD yield of $^{18}O_2$ on $TiO_2(110)$ is shown in Figure 37.[30] A constant amount of $^{18}O_2$ ($^{18}O_2$ exposure 3.8×10^{13} molecules cm^{-2}) was preadsorbed at the $TiO_2(110)$ surface followed by exposing variable amounts of Cl_2 or CH_3OH. Figure 37d plots the initial ESD yield of $^{18}O_2$ (as shown in the dashed circles in Figures 37a, b) as a function of Cl_2 or CH_3OH exposure. The initial rate of $^{18}O_2$ desorption is greatly enhanced by the adsorbed Cl_2, and the full coverage of Cl_2 results in a ~25-fold increase of the $^{18}O_2$ desorption rate. Conversely, the adsorbed CH_3OH decreases the initial rate of $^{18}O_2$ desorption and the decrease continues to zero at high CH_3OH coverage.

As we discussed in section 2.5, the O_2 ESD yield is directly proportional to the surface hole availability. The behavior of Cl_2 and CH_3OH is explained by Figure 36. An electron acceptor, Cl_2, removes electrons from the TiO_2, causing upward-band bending, which promotes the hole availability to the surface. In contrast, CH_3OH donates electrons to the TiO_2 causing downward band bending, which diminishes the hole availability to the surface where either electrons or photons excite the TiO_2.

The O_2 itself is also an electron acceptor. A 2.3-fold enhancement of the $^{18}O_2$ ESD initial yield is observed in Figure 37c when $^{16}O_2$ is coadsorbed ($^{16}O_2$ exposure 1.0×10^{15} molecules cm^{-2}). The dual use of $^{18}O_2$ and $^{16}O_2$ clearly separates electronic effects due to O_2 adsorption from simple coverage effects.

The effect of band bending on the electronically excited oxidation of adsorbed CO has also been investigated on the $TiO_2(110)$ surface.[78] The influence of Cl_2 on the CO oxidation was carried out by exposing various amounts of Cl_2 onto the $TiO_2(110)$ surface following the exposure to a constant amount of $^{18}O_2$ (exposure 3.84×10^{13} molecules cm^{-2}) and to $C^{16}O$ (exposure 1.18×10^{14} molecules cm^{-2}) at 85 K. $C^{16}O^{18}O$, which was detected by the QMS, is produced on the surface through electronically excited oxidation of adsorbed $C^{16}O$ with $^{18}O_2$, using 100 eV electron impact. Figure 38 plots the initial yields of $^{18}O_2$ (upper panel) and $C^{16}O^{18}O$ (lower panel) with

dx.doi.org/10.1021/cr3000626 | *Chem. Rev.* XXXX, XXX, XXX–XXX

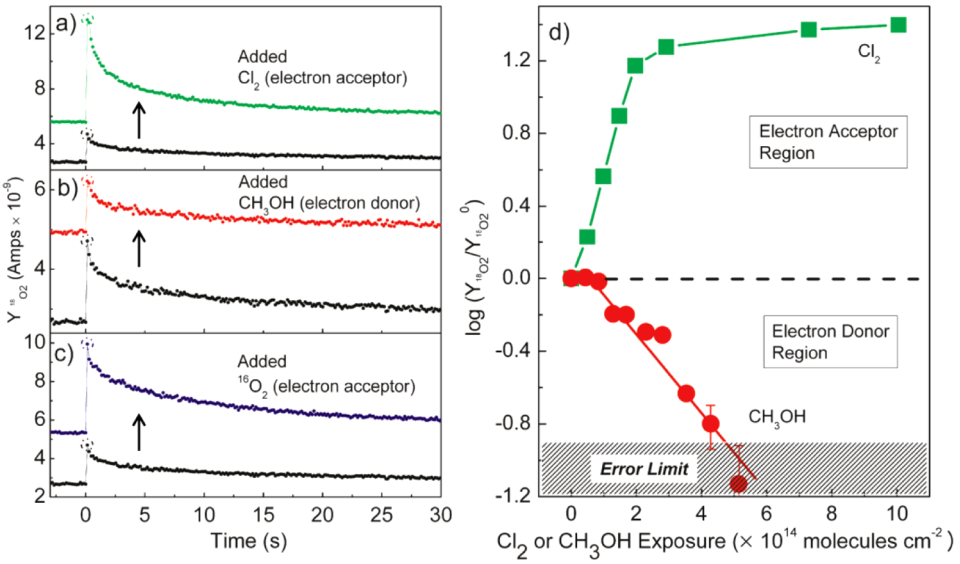

Figure 37. Electron-stimulated desorption (100 eV) measurements by QMS for $^{18}O_2$ on $^{18}O_2/TiO_2(110)$ surfaces in the presence of (a) Cl_2 (green curve, Cl_2 exposure 9.8×10^{13} molecules cm^{-2}), (b) CH_3OH (red curve, CH_3OH exposure 1.3×10^{14} molecules cm^{-2}), and (c) $^{16}O_2$ (blue curve, $^{16}O_2$ exposure 1.0×10^{15} molecules cm^{-2}). The ESD measurement of preadsorbed $^{18}O_2$ ($^{18}O_2$ exposure 3.8×10^{13} molecules cm^{-2}) is also shown in the black curve in parts a, b, and c as a reference. The initial rate of $^{18}O_2$ desorption is measured by the circled point in each case. All the gas dosing and ESD experiments have been done at 85 K. (d) Plots of the initial ESD yield of $^{18}O_2$ as a function of Cl_2 or CH_3OH exposure. The electron bombardment is rapidly initiated at 0 s, and the first point in the O_2 desorption curve is measured within 0.2 s. Reprinted with permission from ref 30. Copyright 2010 American Chemical Society.

various Cl_2 exposures. A significant difference can be found between the $C^{16}O^{18}O$ and the $^{18}O_2$ in the trends of ESD yield as a function of Cl_2 exposure. As we discussed above, Cl_2 is an electron acceptor causing upward band bending and increasing the $^{18}O_2$ ESD yield. In contrast to the increasing yield of $^{18}O_2$, the CO_2 production decreases with the Cl_2 exposure. This can be explained by the model in Figure 39. The O_2 ESD is caused by the interaction between the hole and the adsorbed O_2, while the CO oxidation is mediated by the excited electrons. The adsorbed O_2, usually denoted as O_2^- superoxide species based on theory,[133,220,221] ESR,[217,222] and EELS[223] experiments, can interact with the excited electrons producing the O_2^{2-} species (peroxide ion), which is well-known for its ability to cause oxidation. The upward band bending by Cl_2 inhibits the excited electron transport to the surface and hence decreases the electron-mediated CO oxidation.

3.5.1. Dual Roles of O_2 in CO Oxidation. The influence of the adsorption of O_2 itself on the excited oxidation of CO has been investigated in Figure 40. To do this experiment, the $TiO_2(110)$ surface was first exposed to a constant amount of $C^{16}O$ (exposure 1.18×10^{14} molecules cm^{-2}) followed by exposure to various amounts of $^{18}O_2$. The upper panel in Figure 40 plots the initial yields of $^{18}O_2$ as a function of $^{18}O_2$ exposure. The increase of the $^{18}O_2$ ESD yield with increasing $^{18}O_2$ exposure is due to two effects: (1) increasing O_2 coverage; (2) increasing upward band bending promoting the hole transport to the adsorbed O_2 (Figures 36 and 37). The mix of the above two effects in the CO oxidation produced a volcano curve of CO_2 production in the lower panel of Figure 40. Initially, the yield of CO_2 increases due to the increasing of O_2 coverage. However, at high O_2 coverage, the CO_2 production reaches a maximum and then decreases, which indicates that the upward band bending due to the O_2 adsorption inhibited the CO_2 production. This experiment revealed the dual roles of O_2 in the oxidation of CO: (1) O_2 as a reactant promotes the CO oxidation; (2) O_2 as an electron acceptor causes upward band bending inhibiting the electron-mediated CO oxidation.

3.6. Metal/Semiconductor Band Bending and Photochemistry

Metal/semiconductor heterojunctions have wide application in the field of photochemistry. Band bending due to metal−semiconductor contact can significantly enhance the excited electron−hole separation in semiconductor or metal and hence change the photochemical activity.

3.6.1. Enhancement of Electron−Hole Separation in Semiconductors. The influence of Au on the behavior of photogenerated carriers in $TiO_2(110)$ has been studied by combining a PSD experiment and DFT calculations. Various coverages of Au (0−0.54 ML) were deposited onto a $TiO_2(110)$ surface with a constant coverage of preadsorbed $^{18}O_2$ (exposure 8.64×10^{13} molecules cm^{-2}) to investigate the rate of $^{18}O_2$ PSD by UV light. Figure 41a shows the QMS measurements of the $^{18}O_2$ yield during the UV excitation as a function of the Au deposition, which is similar to the previous ESD experiments (Figures 26 and 37). The initial yield of $^{18}O_2$ as a function of Au coverage on the $TiO_2(110)$ surface is plotted in Figure 41b. Similar to CH_3OH, the presence of Au depresses the initial $^{18}O_2$ PSD yield and ~0.16 ML of Au coverage can decrease the initial yield by 50% as shown by the dashed line. From the discussion of section 3.5, the decrease of $^{18}O_2$ PSD yield indicates the depression of the hole flux to the surface, which means that Au acts as an electron donor bending the energy bands downward. This indicates that the Au atoms acquire positive charge.

The geometrical structures and energy band structures of the $TiO_2(110)$ surface modified by O_2 and O_2 + Au have been studied by DFT calculations as indicated in Figures 42 and 43. DFT calculation shows that O_2 prefers to adsorb at the BBOV site with a bonding energy of approximately −2.3 eV (Figure 42b), and O_2 is negatively charged accepting ~1 e from TiO_2.

dx.doi.org/10.1021/cr3000626 | Chem. Rev. XXXX, XXX, XXX−XXX

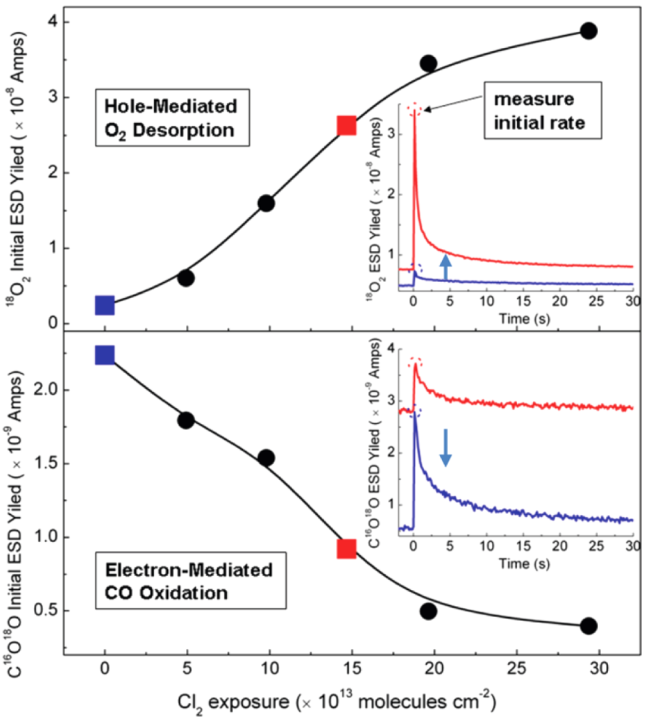

Figure 38. Plots of the initial yield of $^{18}O_2$ (upper panel) and $C^{16}O^{18}O$ (lower panel) as a function of Cl_2 exposure during electronic excitation of a $C^{16}O$ + $^{18}O_2$ mixed layer. Inset shows the measurements by QMS for $^{18}O_2$ (upper panel) and $C^{16}O^{18}O$ (lower panel) yields during electronic excitation in the presence of Cl_2 (blue curve, Cl_2 exposure 0 molecules cm^{-2}; red curve, Cl_2 exposure 1.47× 10^{14} molecules cm^{-2}) on the $C^{16}O^{18}O/^{18}O_2/TiO_2(110)$ surface. $^{18}O_2$ exposure 3.84 × 10^{13} molecules cm^{-2}; $C^{16}O$ exposure 1.18 × 10^{14} molecules cm^{-2}, at 85 K. The electron bombardment is rapidly initiated at 0 s, and the initial desorption yields of $^{18}O_2$ and $C^{16}O^{18}O$ are measured within the first 0.2 s (as shown in the dashed circles in the insets). Reprinted with permission from ref 78. Copyright 2010 American Chemical Society.

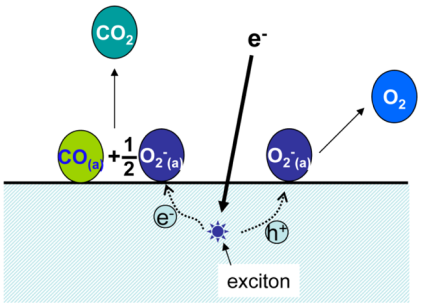

Figure 39. Schematic mechanism of O_2 desorption and CO oxidation on $TiO_2(110)$ during electronic excitation. Desorption of O_2^- as $O_2(g)$ is induced by holes; reaction of O_2^- to produce CO_2 is induced by excited electrons created in the TiO_2. Reprinted with permission from ref 78. Copyright 2010 American Chemical Society.

The energy band structure in Figure 43b indicates that the presence of O_2 on the $TiO_2(110)$ bends the VB and CB edges upward, which corroborates the previous ESD and PES experimental results.[30,44,76−78] There are two favorable sites for a single Au atom on the $O_2/TiO_2(110)$ surface, near the Ti_{5c} site (Figure 42c) and near the BBO site (Figure 42d). An average charge on a single Au atom is approximately +0.2 e based on the two configurations. Contrary to the $^{18}O_2$-induced upward band bending, the adsorption of Au on the $O_2/TiO_2(110)$ surface bends the energy band ~0.6 eV downward, which agrees with the deduction from the PSD experiment.

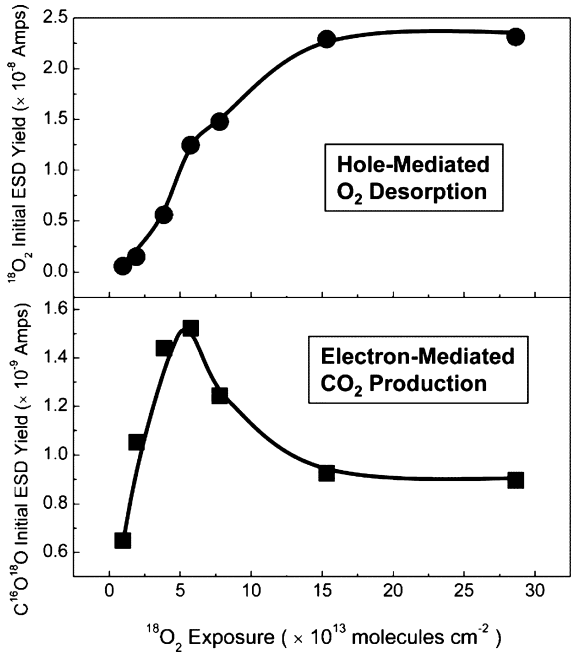

Figure 40. Plots of the initial yields of $^{18}O_2$ (upper panel) and $C^{16}O^{18}O$ (lower panel) as a function of $^{18}O_2$ exposure during electronic excitation of a $C^{16}O$ layer. The preadsorbed $C^{16}O$ exposure is 1.18 × 10^{14} molecules cm^{-2} at 85 K. Reprinted with permission from ref 78. Copyright 2010 American Chemical Society.

Figure 44a gives a schematic diagram of the Au-induced band bending and its effect on hole transport. The presence of downward band bending caused by electropositive Au on the $O_2/TiO_2(110)$ surface depresses the hole transport to the surface and hence the O_2 PSD yield. The Au-induced band bending is equal to the work function change, $\Delta\phi$.

Based on the Topping model,[224] Macdonald and Barlow[225] proposed a model in which ϕ was modified by the self-depolarization of the neighbor adsorbed atoms,

$$\Delta\phi = -4\pi e\mu\theta\sigma/[1 + \alpha\Lambda\delta(\theta\sigma)^{3/2}] \quad (27)$$

where μ is the initial dipole moment induced by the Au adsorption (assuming r_{Au-TiO_2} = 2.6 × 10^{-8} cm), θ is the Au fractional coverage, σ is the saturated Au atom concentration on the $TiO_2(110)$ (1.04 × 10^{15} atoms/cm^2), α is the Au polarizability (5.8 × 10^{-24} cm^3), Λ is a constant (generally equal to 9), $\delta = \theta^{-1/2}$ for immobile Au atoms on $TiO_2(110)$ at 89 K, and e is the elementary charge (4.8 × 10^{-10} esu). According to the Macdonald−Barlow model, the change of the calculated $\Delta\phi$ (blue triangles in Figure 44b) with Au coverage is almost linear, which indicates that the number of electrons transferring from Au to TiO_2 is almost constant.

According to DFT calculation, the average electron transfer from Au to TiO_2 decreases as bigger clusters form statistically as immobile Au atoms are deposited. The average charge of Au monomer, dimer, and trimer clusters are about +0.2 e, +0.1 e, and +0.1 e, respectively, on the $TiO_2(110)$ surface. The increasing Au coverage will statistically decrease the relative population of monomer while increasing the dimer and trimer populations. Consequently, the average charge of the Au atoms will decrease with bigger Au cluster formation. Contrary to the Macdonald−Barlow model, the red squares in Figure 44b

dx.doi.org/10.1021/cr3000626 | Chem. Rev. XXXX, XXX, XXX−XXX

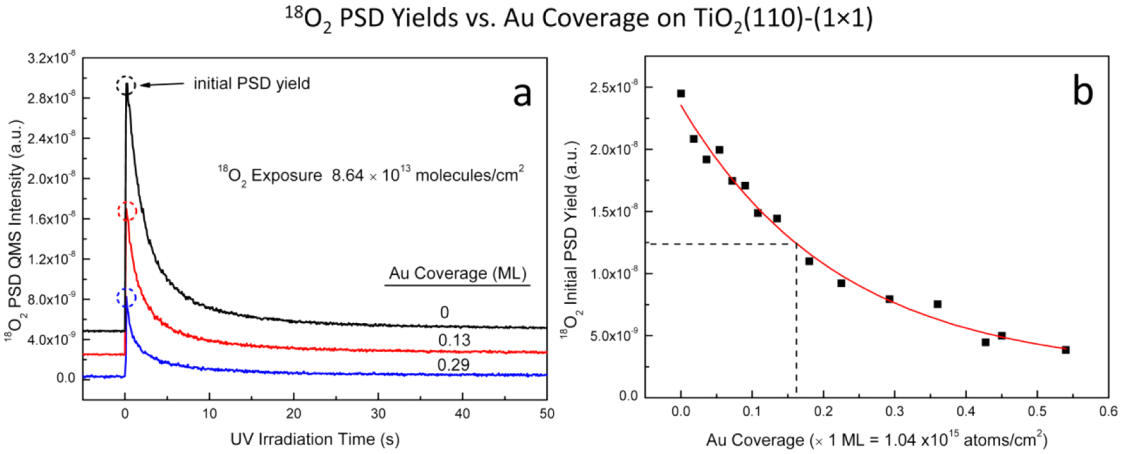

Figure 41. (a) The QMS measurement of the $^{18}O_2$ yields during the UV excitation in the presence of Au (coverages of 0, 0.13, and 0.29 ML) deposited in ultrahigh vacuum on the $^{18}O_2/TiO_2$(110) surface. The initial PSD yields of $^{18}O_2$ are indicated by the dashed circles. (b) A plot of the initial yield of $^{18}O_2$ versus Au coverage on the $^{18}O_2/TiO_2$(110) surface. Reprinted with permission from ref 120. Copyright 2011 American Chemical Society.

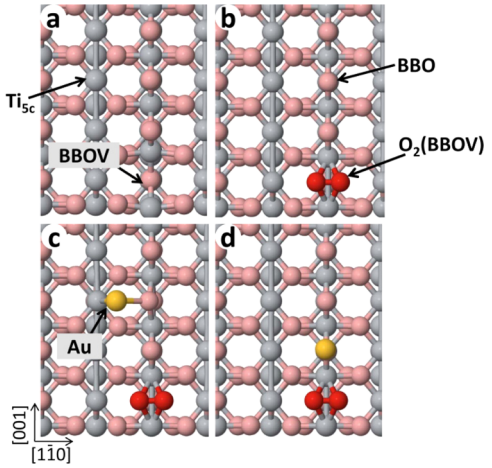

Figure 42. Structural models of (a) the clean TiO_2(110) surface with bridge-bonded oxygen vacancies (BBOVs), (b) TiO_2(110) with O_2 adsorbed at the BBOVs, (c) TiO_2(110) with Au adsorbed near Ti_{5c} sites (the sites between Ti_{5c} and the BBOV site) and O_2 adsorbed on BBOVs; (d) TiO_2(110) with Au adsorbed on BBO and O_2 adsorbed on a vicinal BBOV. The Au atoms and Ti atoms are shown in yellow and gray, respectively, whereas the O in the lattice and adsorbed O are shown in pink and red, respectively. Reprinted with permission from ref 120. Copyright 2011 American Chemical Society.

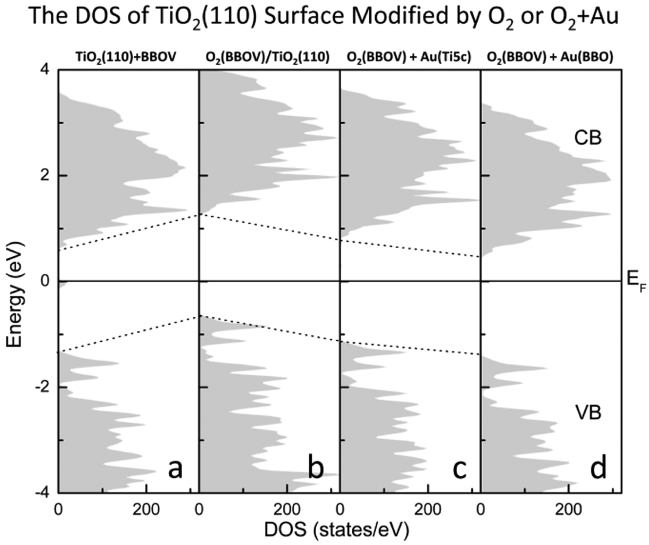

Figure 43. The calculated total DOS of TiO_2(110) with (a) BBOV, (b) O_2 adsorption on BBOV, (c) Au adsorption *near* Ti_{5c} sites (the sites between Ti_{5c} and a BBO site) and O_2 adsorption on BBOV, and (d) Au adsorption on BBO and O_2 adsorption on a vicinal BBOV. The corresponding structural models have been indicated in Figure 42. Reprinted with permission from ref 120. Copyright 2011 American Chemical Society.

showed a more curved plot, which qualitatively correlates with the curvature in $^{18}O_2$ PSD yield for increasing Au coverage (Figure 41). The curvature is therefore mainly due to Au dimer and trimer formation on the surface.

Using STM, the influence of band bending on the photodecomposition of trimethyl acetate (TMA) on the TiO_2(110) surface has also been studied.[226] Figure 45a–d shows the STM images of TMA photodecomposition on the Pt/TiO_2(110) surface (Figure 45a,b) and the TiO_2(110) surface (Figure 45c,d) surfaces. The coverages of TMA on the Pt/TiO_2(110) after 1 h (Figure 45a) and 3 h (Figure 45b) UV photoirradiation are significantly lower than that on the clean TiO_2(110) surface. That indicates that the presence of 3–4 nm Pt particles (big bright spots in Figure 45a,b) can significantly enhance the decomposition rate of TMA. From the statistical studies of many STM images, Figure 45e plots the TMA coverages as a function of UV light irradiation time on a TiO_2(110) surface covered with (a) 0, (b) 3 × 10^{15}, and (c) 8 × 10^{15} particles m^{-2}, which corroborate the results shown in Figure 45a–d. It is believed that the decomposition of TMA is caused by the photogenerated holes in TiO_2. That means the presence of negatively charged Pt can significantly enhance the hole transport from TiO_2 substrate to adsorbed TMA. The mechanism is indicated in Figure 45f, which is similar to the Cl_2 and O_2 effect as we discussed before. It should be mentioned that the same group later found that Pt clusters donate electrons to the TiO_2 substrate using Kelvin probe force microscope on the Pt/TiO_2(110) surface without TMA.[227] It is possible that the presence of TMA on TiO_2(110) surface may decrease or reverse the direction of electron transfer and change the Pt clusters from an electron donor to an electron acceptor. Previous DFT calculation and experimental re-

dx.doi.org/10.1021/cr3000626 | *Chem. Rev.* XXXX, XXX, XXX–XXX

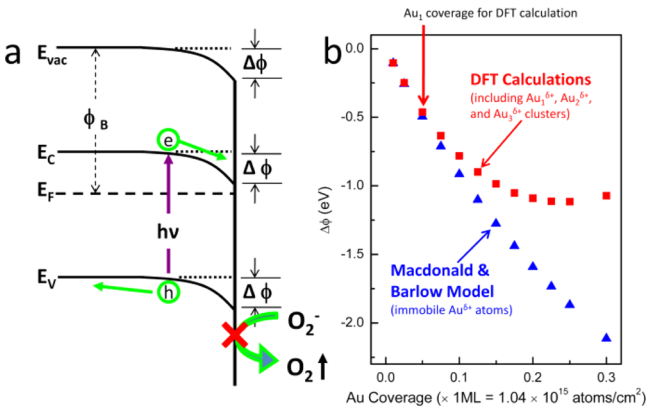

Figure 44. (a) Schematic diagram of downward band bending by Au and its effect on hole transport causing decreasing $^{18}O_2$ PSD yield. (b) The plots of the work function change calculated by DFT and the Macdonald and Barlow model vs Au coverage on $^{18}O_2/TiO_2(110)$ surface. Reprinted with permission from ref 120. Copyright 2011 American Chemical Society.

sults[120,228,229] indicated that the presence of oxygen can turn the negative charged Au clusters on a clean (reduced) $TiO_2(110)$ surface to positive charged clusters.

3.6.2. Enhancement of Electron–Hole Separation in Metals. The excited electron–hole pairs in the metal can also be separated by the metal/semiconductor heterojunction. For example, in section 1.3.2 (Figure 11c), the electrons excited by chemical reactions on metal surfaces with energy higher than ϕ_{SB} are postulated to transfer from the metal to the semiconductor causing a chemicurrent. Recently, the hot electrons from the photoexcited surface plasmon resonance (SPR) in metal has also been detected in a nano-metal/semiconductor diode.[230,231]

On the other hand, the separated electrons and holes can participate in the chemical reactions on the metal and semiconductor surfaces. A diagram showing the surface plasmon resonance induced charge transfer and reaction is shown in Figure 46. The valence electrons in the metal particles

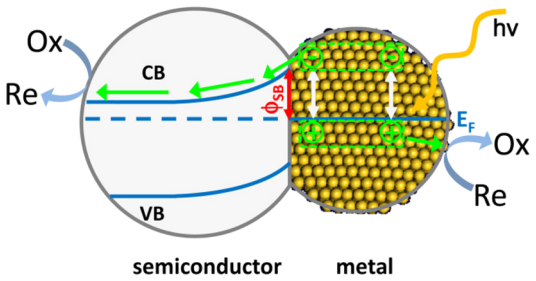

Figure 46. Schematic diagram of plasmon-induced charge separation and associated photochemistry at the metal/semiconductor heterojunction. Here the electron charge separated in the metal is transferred to the semiconductor. An alternate mechanism involving an electrodynamic model is also postulated.[12]

can be collectively excited by the absorption of photons, which is called a surface plasmon resonance. The excited electrons with energy higher than ϕ_{SB} can cross the metal/semiconductor interface and transfer to the valence band of the semiconductor. This mechanism and the influence of barrier height and width on the electron–hole separation are similar to the dye-sensitization process, which was discussed in section 3.1.2.1. Oxidation (reduction) reactions may occur on the metal

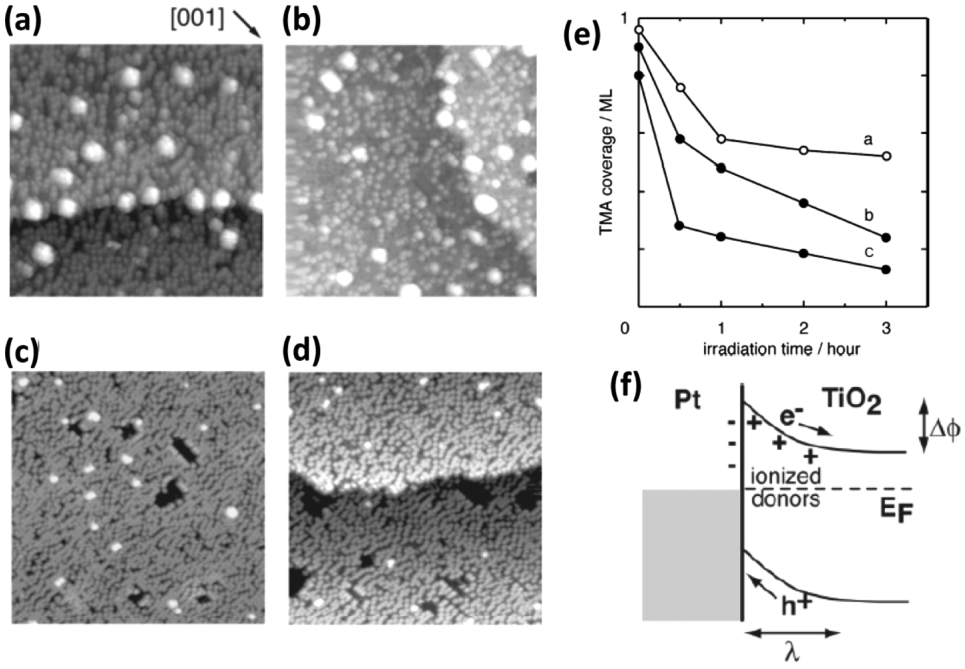

Figure 45. (a–d) Constant current STM images of TMA photodecomposed on the $Pt/TiO_2(110)$ and $TiO_2(110)$ surface. The Pt-modified surface was exposed to 100 L of trimethylacetic acid and then UV irradiated for (a) 1 h and (b) 3 h. A TMA-covered, Pt-free $TiO_2(110)$ surface was irradiated with the same UV flux for (c) 1 h and (d) 3 h for comparison. Image size: 40 × 40 nm^2. Sample bias voltage: +1.6 V. Tunnel current: 0.4 nA. (e) The TMA coverages as a function of UV light irradiation time on a $TiO_2(110)$ surface covered with (a) 0, (b) 3 × 10^{15}, and (c) 8 × 10^{15} Pt particles m^{-2}. (f) Schematic diagram of the influence of Pt on the photoexcited carrier transfer in TiO_2. Reprinted with permission from ref 226. Copyright 2005 American Chemical Society.

dx.doi.org/10.1021/cr3000626 | *Chem. Rev.* XXXX, XXX, XXX–XXX

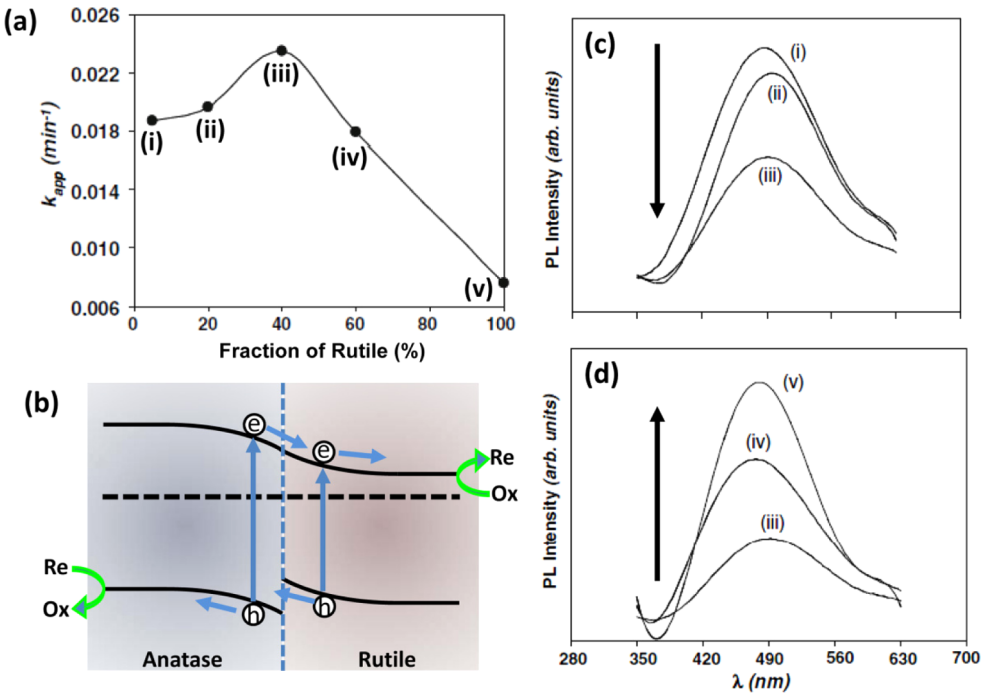

Figure 47. (a) Variation of photodegradation activity of methylene blue (k_{app}) in solution as a function of rutile fraction in mixed-phase TiO_2 (anatse +rutile), (b) proposed interface band bending model between anatase and rutile, and (c, d) typical PL spectra obtained for the mixed-phase nanocrystalline TiO_2 for rutile content within the range of (c) 5−40 wt % and (d) 40−100 wt %. In panels a, c, and d, i−v denote rutile fractions of 5, 20, 40, 60, and 100 wt %, respectively. Adapted with permission from refs 245 and 247 Copyright 2011 Elsevier and 2009 Springer.

(semiconductor) surface with the separated holes (electrons) in this case.

By changing the composition, shape, and size of the metal particles,[232−234] the surface plasmon resonance frequency of metal particle can be tuned in the visible spectrum range, which may have potential application in harvesting sunlight.[12,235−239] For example, a notable visible-light photocatalytic activity of a Au/TiO_2 surface on the photolysis of water has been discovered. Silva et al.[236] proposed that the electrons in the metal can be injected to the TiO_2 conduction band due to the surface plasmon resonance by visible light, leaving holes in the Au particles. Water can react with the electrons in the TiO_2 producing hydrogen and react with the Au particles producing oxygen. It should be mentioned that besides the charge transfer metal/semiconductor mechanism, there is also an electrodynamic mechanism for the surface plasmon resonance effect during the photochemistry processes, which is discussed in an article by Linic et al.[12]

3.7. Semiconductor/Semiconductor Band Bending and Photochemistry

The synergetic effect between complex semiconductor catalysts has been widely observed in photochemical reactions.[240−244] During the photocatalytic process, the presence of another semiconductor cocatalyst may provide special active sites for the adsorption/reaction of reactants/reaction intermediates. A second semiconductor can also modify the composite band structure helping to change the bandgap absorption and to separate the photoexcited electron−hole pairs.

In this section, we focus on the band bending effect between the cocatalyst semiconductors and its influence on the photocatalytic processes. The band bending between two semiconductors can be influenced by many factors such as doping type and concentration, particle size, surface structure, phase, etc. Herein, we will discuss the synergetic effect between rutile and anatase TiO_2 caused by band bending. It is well-known that usually the complex catalyst consisting of the mixed phase of anatase and rutile (such as P25 TO_2 powder) presents higher photocatalytic activity than pure rutile and anatase.[241,245−248] Baiju et al.[247] studied the photodegradation of methylene blue dye by a mixed phase of rutile and anatase TiO_2 under UV light irradiation. As shown in Figure 47a, the photocatalytic activity (apparent rate constant of photodegradation, k_{app}) first increases as the rutile fraction increases and then reaches a maximum at 40% rutile. After that, photoactivity decreases with increasing rutile fraction. The rutile fraction-dependent photoactivity of the mixed TiO_2 catalyst can be well explained by the band bending model in Figure 47b. From previous Kelvin probe, PEEM, and UPS studies,[249,250] the work function of anatase is a little higher than that of rutile, which causes the energy bands of anatase to bend downward and rutile to bend upward toward the interface after the two phases are in contact and to reach electrical equilibrium. The presence of an electric field near the interface effectively separates the electron−hole pair and inhibits the electron−hole pair recombination. The mixed phase catalyst with highest photocatalytic activity (40% rutile amount) is postulated to have the maximum anatase/rutile interfacial contact and the most effective electron−hole pair separation.

As discussed in sections 2.2 and 2.3, PL spectroscopy offeres an effective way for investigating the band bending and electron−hole pair separation. Figure 47c,d shows the PL spectra obtained for the mixed-phase TiO_2 with different rutile content. The sample with 40% rutile content presents the lowest PL intensity at ~490 nm indicating the least electron−hole recombination, which agrees with the reaction data. The electron transfer from anatase to rutile has also been observed

dx.doi.org/10.1021/cr3000626 | Chem. Rev. XXXX, XXX, XXX−XXX

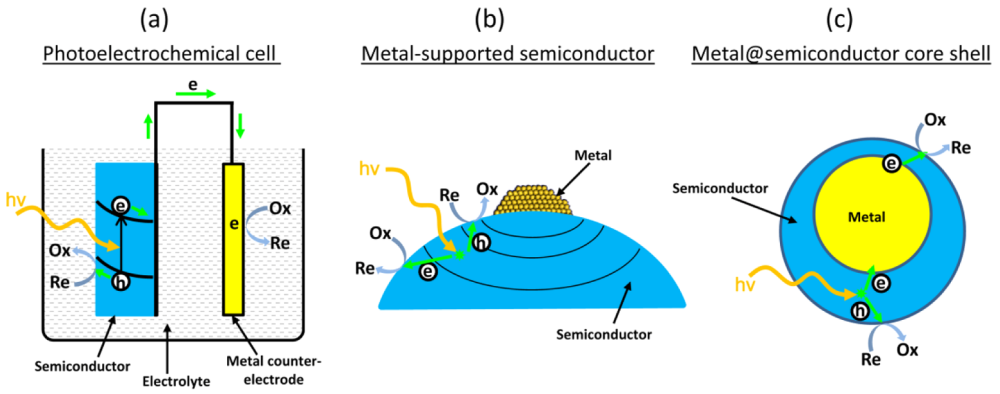

Figure 48. Three metal/semiconductor photocatalytic systems: (a) photoelectrochemical cell; (b) metal particle supported on semiconductor; (c) metal@semiconductor core shell.

by Kawahara et al.[251] on a patterned TiO_2(anatase)/TiO_2(rutile) bilayer-type photocatalyst.

3.8. Band Bending in a Real Photocatalytic System

The manifestation of band bending in photocatalysts has been discussed above from a microscopic viewpoint. The presence of band bending can significantly depress the electron–hole pair recombination rate and enhance the migration rates of one charge carrier (electron or hole) to the semiconductor surface, which may enhance the corresponding charge carrier (electron/hole) mediated reaction on the semiconductor surface. Meanwhile, the inverse charge carriers (hole/electron) may transfer beyond the space charge region in the other direction and should also be depleted to keep the photocatalyst neutral and maintain the band bending in the semiconductor. Here we discuss the depletion of both photogenerated charge carriers in a real photocatalytic system.

Taking a metal/semiconductor system as an example, three metal/semiconductor catalyst systems can be found in the real photocatalytic reactions discussed in Figure 48:

(1) Photoelectrochemical cell. In the photoelectrochemical cell system with upward band bending near the semiconductor/electrolyte interface (Figure 48a), the photogenerated holes will transfer to the semiconductor/electrolyte interface and a reduction reaction occurs, while the photogenerated electrons will transfer to the metal counterelectrode. An oxidative reaction occurs at the semiconductor/electrolyte interface.[2,12,252]

(2) Metal-supported semiconductor particles. Figure 48b shows the model of the metal-supported semiconductor photocatalyst with downward band bending near the metal/semiconductor contact. The photogenerated electron–hole pair can be separated effectively by the local electric field near the metal particles. The photogenerated holes will be enriched near or on the metal particles causing oxidation reactions, while the photogenerated electrons may transfer out of the space charge layer causing a reduction reaction.[253]

(3) Metal@semiconductor core–shell particles. Compared with the metal-supported semiconductor photocatalyst, the metal@semiconductor core–shell structure photocatalyst can significantly eliminate the corrosion or dissolution of metal particles on metal-supported semiconductor surfaces during the photocatalytic processes.[254] As shown in Figure 48c, there may be band bending near the interface between metal core and semiconductor shell, which may separate the excited electron–hole pair in the semiconductor effectively. The charge separation and photocatalytic activity of a Ag@TiO_2 core–shell structure has been studied by Hirakawa and Kamat.[255,256] The electrons transferred from the semiconductor to the metal core under UV illumination (excitation in TiO_2) can be quantitatively measured by the shift of the surface plasmon band. The electrons stored in the metal core can transfer outside to reduce electron acceptor molecules such as O_2, thionine, or C_{60}.[255]

4. SUMMARY

The subject of band bending in semiconductors, caused chemically or by means of applied electric fields, has a wide and general application for the understanding of photoprocesses as well as for the control of the efficiency in charge transfer from the excited semiconductor to the external world. From the fundamental physics of semiconductor behavior upon excitation by photons to the utilization of photogenerated charge carriers in electronic or chemical devices, the concept of band bending is useful for the prediction of the behavior and the control of photon-energy conversion devices. The band bending concept provides a useful and predictive way for the utilization of semiconductors for converting incident photons into useful electrical energy or useful chemistry. While this concept is widespread in solid-state physics, the extension to much of the chemistry world lags behind, forming the stimulus for writing this review.

AUTHOR INFORMATION

Corresponding Author

*E-mail: johnt@virginia.edu.

Notes

The authors declare no competing financial interest.

dx.doi.org/10.1021/cr3000626 | *Chem. Rev.* XXXX, XXX, XXX–XXX

Biographies

Zhen Zhang was born in Jiangsu, China. He received his B.S. degree in Chemistry from Nanjing University, China, in 2001. Then, he entered Dalian Institute of Chemical Physics, the Chinese Academy of Sciences, and completed his Ph.D. degree with a thesis on ultrahigh vacuum surface science and model catalysis under the supervision of Professor Xinhe Bao. Afterwards, he became a postdoctoral fellow at University of Virginia under the directorship of Professor John T. Yates, Jr., since 2008. His current research interests include electronic excitation and surface chemistry on metal oxide surfaces.

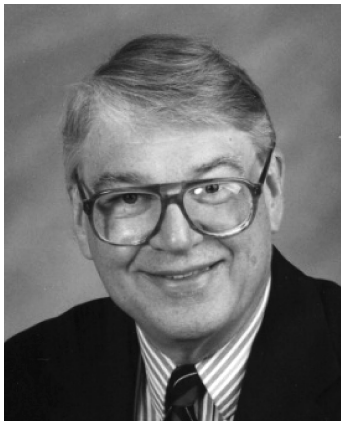

John T. Yates, Jr., is a physical chemist specializing in the field of surface chemistry. He has spent 30 years in academia, first as R. K. Mellon Professor and founding Director of the Surface Science Center at the University of Pittsburgh (Departments of Chemistry and Physics) and lately as Shannon Research Fellow and Professor at the University of Virginia (Departments of Chemistry and Chemical Engineering). Prior to his academic experiences, he was a research staff member at National Bureau of Standards (now National Institute of Standards and Technology) in the Physical Chemistry Division. His work has encompassed many aspects of surface chemistry through experimental studies of the properties of adsorbed layers on metals, semiconductors, and insulators using advanced measurement methods. He is the author of more than 700 research publications, several books, and a number of reviews. He is the winner of a number of professional awards in the ACS and the AVS. In 1995, he was elected to the National Academy of Sciences.

ACKNOWLEDGMENTS

We acknowledge, with thanks, the support of the DOE Office of Basic Energy Sciences under Grant Number DE-FG02-09ER16080. We also acknowledge partial support by the Army Research Office under Grant Number 55748CH.

REFERENCES

(1) Yates, J. T., Jr.; Petek, H. *Chem. Rev.* **2006**, *106*, 4113.
(2) Fujishima, A.; Honda, K. *Nature* **1972**, *238*, 37.
(3) Fox, M. A.; Dulay, M. T. *Chem. Rev.* **1993**, *93*, 341.
(4) Mills, A.; Davies, R. H.; Worsley, D. *Chem. Soc. Rev.* **1993**, *22*, 417.
(5) Hoffmann, M. R.; Martin, S. T.; Choi, W. Y.; Bahnemann, D. W. *Chem. Rev.* **1995**, *95*, 69.
(6) Linsebigler, A.; Lu, G. Q.; Yates, J. T., Jr. *Chem. Rev.* **1995**, *95*, 735.
(7) Thompson, T. L.; Yates, J. T., Jr. *Chem. Rev.* **2006**, *106*, 4428.
(8) Matsuoka, M.; Kitano, M.; Takeuchi, M.; Tsujimaru, K.; Anpo, M.; Thomas, J. M. *Catal. Today* **2007**, *122*, 51.
(9) Kamat, P. V. *J. Phys. Chem. C* **2007**, *111*, 2834.
(10) Chen, X. B.; Shen, S. H.; Guo, L. J.; Mao, S. S. *Chem. Rev.* **2010**, *110*, 6503.
(11) Henderson, M. A. *Surf. Sci. Rep.* **2011**, *66*, 185.
(12) Linic, S.; Christopher, P.; Ingram, D. B. *Nat. Mater.* **2011**, *10*, 911.
(13) Tung, R. *Mater. Sci. Eng., R* **2001**, *35*, 1.
(14) Sze, S. M.; Ng, K. K. *Physics of Semiconductor Devices*, 3rd ed.; John Wiley & Sons, Inc.: Hoboken, NJ, 2007.
(15) Gerischer, H. *Surf. Sci.* **1969**, *18*, 97.
(16) Gerischer, H. *Electrochim. Acta* **1990**, *35*, 1677.
(17) Bard, A. J. *J. Photochem.* **1979**, *10*, 59.
(18) Göpel, W.; Schierbaum, K. D. *Sens. Actuators, B* **1995**, *26–27*, 1.
(19) Barsan, N.; Weimar, U. *J. Electroceram.* **2001**, *7*, 143.
(20) Schottky, W. *Z. Phys.* **1939**, *113*, 367.
(21) Schottky, W. *Naturwissenschaften* **1938**, *26*, 843.
(22) Mott, N. F. *Proc. R. Soc. London, Ser. A* **1939**, *171*, 27.
(23) Mott, N. F. *Proc. Cambridge Philos. Soc.* **1938**, *34*, 568.
(24) Bardeen, J. Nobel Lecture December 11, 1956.
(25) McEllistrem, M.; Haase, G.; Chen, D.; Hamers, R. J. *Phys. Rev. Lett.* **1993**, *70*, 2471.
(26) Ma, X. Y.; Chen, P. L.; Li, D. S.; Zhang, Y. Y.; Yang, D. R. *Appl. Phys. Lett.* **2007**, *91*, No. 021105.
(27) Ghosh, M.; Raychaudhuri, A. K. *Appl. Phys. Lett.* **2011**, *98*, No. 153109.
(28) Zangwill, A. *Physics at Surfaces*; Cambridge University Press: New York, 1988.
(29) Brillson, L. J. *Surf. Sci. Rep.* **1982**, *2*, 123.
(30) Zhang, Z.; Yates, J. T., Jr. *J. Phys. Chem. Lett.* **2010**, *1*, 2185.
(31) Lüth, H. *Solid Surfaces, Interfaces and Thin Films*, 5th ed.; Springer: New York, 2010.
(32) Grätzel, M. *Nature* **2001**, *414*, 338.
(33) Ioannides, T.; Verykios, X. E. *J. Catal.* **1996**, *161*, 560.
(34) Smit, G. D. J.; Rogge, S.; Klapwijk, T. M. *Appl. Phys. Lett.* **2002**, *81*, 3852.
(35) Zhdanov, V. P.; Kasemo, B. *Physica E* **2011**, *43*, 1486.
(36) Zhdanov, V. P. *Surf. Sci.* **2002**, *512*, L331.
(37) Ioannides, T. *Surf. Sci.* **2003**, *530*, 216.
(38) Zhdanov, V. P. *Surf. Sci.* **2003**, *530*, 219.
(39) Donolato, C. *J. Appl. Phys.* **2004**, *95*, 2184.
(40) Miyano, K. E.; King, D. M.; Spindt, C. J.; Kendelewicz, T.; Cao, R.; Yu, Z. P.; Lindau, I.; Spicer, W. E. *Phys. Rev. B* **1991**, *43*, 11806.
(41) Schlaf, R.; Klein, A.; Pettenkofer, C.; Jaegermann, W. *Phys. Rev. B* **1993**, *48*, 14242.
(42) Pitters, J. L.; Dogel, I. A.; Wolkow, R. A. *ACS Nano* **2011**, *5*, 1984.
(43) Ebert, P.; Heinrich, M.; Simon, M.; Urban, K.; Lagally, M. G. *Phys. Rev. B* **1995**, *51*, 9696.
(44) Wendt, S.; Sprunger, P. T.; Lira, E.; Madsen, G. K. H.; Li, Z. S.; Hansen, J. Ø.; Matthiesen, J.; Blekinge-Rasmussen, A.; Lægsgaard, E.; Hammer, B.; Besenbacher, F. *Science* **2008**, *320*, 1755.
(45) Zhang, Z.; Lee, J.; Yates, J. T., Jr.; Bechstein, R.; Lira, E.; Hansen, J. Ø.; Wendt, S.; Besenbacher, F. *J. Phys. Chem. C* **2010**, *114*, 3059.

(46) Lira, E.; Wendt, S.; Huo, P. P.; Hansen, J. Ø.; Streber, R.; Porsgaard, S.; Wei, Y. Y.; Bechstein, R.; Lægsgaard, E.; Besenbacher, F. *J. Am. Chem. Soc.* **2011**, *133*, 6529.
(47) Benz, L.; Haubrich, J.; Quiller, R. G.; Jensen, S. C.; Friend, C. M. *J. Am. Chem. Soc.* **2009**, *131*, 15026.
(48) Bonanni, S.; Ait-Mansour, K.; Brune, H.; Harbich, W. *ACS Catal.* **2011**, *1*, 385.
(49) Cabrera, N.; Mott, N. F. *Rep. Prog. Phys.* **1949**, *12*, 163.
(50) Fromhold, A. T., Jr.; CooK, E. L. *Phys. Rev.* **1967**, *158*, 600.
(51) Fromhold, A. T., Jr.; CooK, E. L. *Phys. Rev.* **1967**, *163*, 650.
(52) Atkinson, A. *Rev. Mod. Phys.* **1985**, *57*, 437.
(53) Guise, O.; Levy, J.; Yates, J. T., Jr. *Thin Solid Films* **2006**, *496*, 426.
(54) Popova, I.; Zhukov, V.; Yates, J. T., Jr. *Phys. Rev. Lett.* **2002**, *89*, No. 276101.
(55) Fu, Q.; Wagner, T. *J. Phys. Chem. B* **2005**, *209*, 11697.
(56) Fu, Q.; Wagner, T. *Surf. Sci. Rep.* **2007**, *62*, 431.
(57) Fu, Q.; Wagner, T.; Olliges, S.; Carstanjen, H.-D. *J. Phys. Chem. B* **2005**, *109*, 944.
(58) Ertl, G. *Reactions at Solid Surfaces*; John Wiley & Sons, Inc.: Hoboken, NJ, 2009.
(59) Nienhaus, H. *Surf. Sci. Rep.* **2002**, *45*, 1.
(60) Nørskov, J. K.; Newns, D. M.; Lundqvist, B. I. *Surf. Sci.* **1979**, *80*, 179.
(61) Greber, T.; Freihube, K.; Grobecker, R.; Böttcher, A.; Hermann, K.; Ertl, G.; Fick, D. *Phys. Rev. B* **1994**, *50*, 8755.
(62) Kasemo, B. *Phys. Rev. Lett.* **1974**, *32*, 1114.
(63) Nienhaus, H.; Bergh, H. S.; Gergen, B.; Majumdar, A.; Weinberg, W. H.; McFarland, E. W. *Phys. Rev. Lett.* **1999**, *82*, 446.
(64) Gergen, B.; Nienhaus, H.; Weinberg, W. H.; McFarland, E. W. *Science* **2001**, *294*, 2521.
(65) Glass, S.; Nienhaus, H. *Phys. Rev. Lett.* **2004**, *93*, No. 168302.
(66) Ji, X. Z.; Zuppero, A.; Gidwani, J. M.; Somorjai, G. A. *Nano Lett.* **2005**, *5*, 753.
(67) Ji, X. Z.; Zuppero, A.; Gidwani, J. M.; Somorjai, G. A. *J. Am. Chem. Soc.* **2005**, *127*, 5792.
(68) Somorjai, G. A. *Catal. Lett.* **2005**, *101*, 1.
(69) Park, J. Y.; Somorjai, G. A. *ChemPhysChem* **2006**, *7*, 1409.
(70) Park, J. Y.; Renzas, J. R.; Hsu, B. B.; Somorjai, G. A. *J. Phys. Chem. C* **2007**, *111*, 15331.
(71) Renzas, J. R.; Somorjai, G. A. *J. Phys. Chem. C* **2010**, *114*, 17660.
(72) Creighton, J. R.; Coltrin, M. E. *J. Phys. Chem. C* **2012**, *116*, 1139.
(73) Horn, K. *Appl. Phys. A: Mater. Sci. Process.* **1990**, *51*, 289.
(74) Hansson, G. V.; Uhrberg, R. I. G. *Surf. Sci. Rep.* **1988**, *9*, 197.
(75) Gao, Y. L. *Mater. Sci. Eng. R* **2010**, *68*, 39.
(76) Diebold, U. *Surf. Sci. Rep.* **2003**, *48*, 53.
(77) Porsgaard, S.; Jiang, P.; Borondics, F.; Wendt, S.; Liu, Z.; Bluhm, H.; Besenbacher, F.; Salmeron, M. *Angew. Chem., Int. Ed.* **2011**, *50*, 2266.
(78) Zhang, Z.; Yates, J. T., Jr. *J. Am. Chem. Soc.* **2010**, *132*, 12804.
(79) Long, J. P.; Bermudez, V. M. *Phys. Rev. B* **2002**, *66*, No. 121308.
(80) Chen, Z. H.; Eich, D.; Reuscher, G.; Waag, A.; Fink, R.; Umbach, E. *Phys. Rev. B* **1999**, *60*, 8915.
(81) Wu, C.-I.; Lee, G.-R.; Pi, T. W. *Appl. Phys. Lett.* **2005**, *87*, No. 212108.
(82) Tisdale, W. A.; Muntwiler, M.; Norris, D. J.; Aydil, E. S.; Zhu, X. Y. *J. Phys. Chem. C* **2008**, *112*, 14682.
(83) Weinelt, M.; Kutschera, M.; Schmidt, R.; Orth, C.; fauster, T.; Rohlfing, M. *Appl. Phys. A: Mater. Sci. Process.* **2005**, *80*, 995.
(84) Gao, Y. L.; Ding, H. J.; Wang, H. B.; Yan, D. H. *Appl. Phys. Lett.* **2007**, *91*, No. 142112.
(85) Hu, Y. J.; Wagener, T. J.; Jost, M. B.; Weaver, J. H. *J. Vac. Sci. Technol. B* **1990**, *8*, 1001.
(86) Nirmal, M.; Brus, L. *Acc. Chem. Res.* **1999**, *32*, 407.
(87) Anpo, M.; Che, M. *Adv. Catal.* **1999**, *44*, 119.
(88) Gfroerer, T. H. Photoluminescence in Analysis of Surfaces and Interfacse. In *Encyclopedia of Analytical Chemistry*; Meyers, R. A., Ed.; John Wiley & Sons Ltd.: Chichester, U.K., 2000.
(89) Sailor, M. J.; Lee, E. J. *Adv. Mater.* **1997**, *9*, 783.
(90) Shi, J. Y.; Chen, J.; Feng, Z. C.; C., T.; Lian, Y. X.; Wang, X. L.; Li, C. *J. Phys. Chem. C* **2007**, *111*, 693.
(91) Yu, P. Y.; Cardona, M. *Fundamentals of Semiconductrs: Physics and Materials Properties*; Springer: New York, 2005.
(92) Shockley, W.; Read, W. T. *Phys. Rev.* **1952**, *87*, 835.
(93) Hall, R. N. *Phys. Rev.* **1952**, *87*, 387.
(94) Mettler, K. *Appl. Phys.* **1977**, *12*, 75.
(95) Anpo, M.; Tomonari, M.; Fox, M. A. *J. Phys. Chem.* **1989**, *93*, 7300.
(96) Anpo, M.; Chiba, K.; Tomonari, M.; Coluccia, S.; Che, M.; Fox, M. A. *Bull. Chem. Soc. Jpn.* **1991**, *64*, 543.
(97) Hollingsworth, R. E.; Sites, J. R. *J. Appl. Phys.* **1982**, *53*, 5357.
(98) Meyer, G. J.; Lisensky, G. C.; Ellis, A. B. *J. Am. Chem. Soc.* **1988**, *110*, 4914.
(99) Stevanovic, A.; Büttner, M.; Zhang, Z.; Yates, J. T., Jr. *J. Am. Chem. Soc.* **2012**, *134*, 324.
(100) Idriss, H.; Andrews, R. M.; Barteau, M. A. *J. Vac. Sci. Technol. A* **1993**, *11*, 209.
(101) Brattain, W. H. *Phys. Rev.* **1947**, *72*, 345.
(102) Brattain, W. H.; Bardeen, J. *Bell Syst. Tech. J.* **1953**, *32*, 1.
(103) Sell, K.; Barke, I.; Polei, S.; Schumann, C.; von Oeynhausen, V.; Meiwes-Broer, K.-H. *Phys. Status Solidi B* **2010**, *247*, 1087.
(104) Kronik, L.; Shapira, Y. *Surf. Sci. Rep.* **1999**, *37*, 1.
(105) Streicher, F.; Sadewasser, S.; Lux-Steiner, M. C. *Rev. Sci. Instrum.* **2009**, *80*, No. 013907.
(106) Higashi, G. S.; Chabal, Y. J.; Trucks, G. W.; Raghavachari, K. *Appl. Phys. Lett.* **1990**, *56*, 656.
(107) Hamers, R. J.; Tromp, R. M.; Demuth, J. E. *Phys. Rev. Lett.* **1986**, *56*, 1972.
(108) Rothschild, A.; Levakov, A.; Shapira, Y.; Ashkenasy, N.; Komem, Y. *Surf. Sci.* **2003**, *532*−*535*, 456.
(109) Dev, K.; Seebauer, E. G. *Surf. Sci.* **2005**, *583*, 80.
(110) Cardona, M.; Shaklee, K. L.; Pollak, F. H. *Phys. Rev.* **1967**, *154*, 696.
(111) Carlson, C. R.; Buechter, W. F.; Che-Ibrahim, F.; Seebauer, E. G. *J. Chem. Phys.* **1993**, *99*, 7190.
(112) Stroscio, J. A.; Feenstra, R. M.; Fein, A. P. *Phys. Rev. Lett.* **1987**, *58*, 1668.
(113) Hamers, R. J. *J. Vac. Sci. Technol. B* **1988**, *6*, 1462.
(114) Binning, G.; Rohrer, H. *Surf. Sci.* **1983**, *126*, 236.
(115) Lang, N. D. *Phys. Rev. B* **1988**, *37*, 10395.
(116) Chen, C. J. *Introduction to Scanning Tunneling Microscopy*; Oxford University Press: New York, 1993.
(117) Weimer, M.; Kramar, J.; Baldeschwieler, J. D. *Phys. Rev. B* **1989**, *39*, 5572.
(118) Ostermann, D.; Walther, G.; Schierbaum, K. D. *Phys. Rev. B* **2005**, *71*, No. 235416.
(119) Maeda, Y.; Okumura, M.; Tsubota, S.; Kohyama, M.; Haruta, M. *Appl. Surf. Sci.* **2004**, *222*, 409.
(120) Zhang, Z.; Tang, W. J.; Neurock, M.; Yates, J. T., Jr. *J. Phys. Chem. C* **2011**, *115*, 23848.
(121) Kaiser, W. J.; Bell, L. D. *Phys. Rev. Lett.* **1988**, *60*, 1406.
(122) Bell, L. D.; Kaiser, W. J. *Phys. Rev. Lett.* **1988**, *61*, 2368.
(123) Crowell, C. R.; Spitzer, W. G.; Howarth, L. E.; LaBate, E. E. *Phys. Rev.* **1962**, *127*, 2006.
(124) Prietsch, M. *Phys. Rep.* **1995**, *253*, 163.
(125) Narayanamurti, V.; Kozhevnikov, M. *Phys. Rep.* **2001**, *349*, 447.
(126) Yi, W.; Stollenwerk, A. J.; Narayanamurti, V. *Surf. Sci. Rep.* **2009**, *64*, 169.
(127) Lu, G. Q.; Linsebigler, A.; Yates, J. T., Jr. *J. Chem. Phys.* **1995**, *102*, 4657.
(128) Thompson, T. L.; Yates, J. T., Jr. *J. Phys. Chem. B* **2005**, *109*, 18230.
(129) Thompson, T. L.; Yates, J. T., Jr. *J. Phys. Chem. B* **2006**, *110*, 7431.
(130) Sporleder, D.; Wilson, D. P.; White, M. G. *J. Phys. Chem. C* **2009**, *113*, 13180.
(131) Perkins, C. L.; Henderson, M. A. *J. Phys. Chem. B* **2001**, *105*, 3856.

(132) Petrik, N. G.; Kimmel, G. A. *J. Phys. Chem. Lett.* **2010**, *1*, 1758.
(133) de Lara-Castells, M. P.; Krause, J. L. *J. Chem. Phys.* **2003**, *118*, 5098.
(134) Zhang, Z.; Yates, J. T., Jr. *J. Phys. Chem. C* **2010**, *114*, 3098.
(135) Geurts, J. *Surf. Sci. Rep.* **1993**, *18*, 1.
(136) Arens, M.; Kinsky, J.; Richter, W.; Eberl, K. *Surf. Sci.* **1996**, *352−354*, 740.
(137) Lorenz, P.; Haensel, T.; Gutt, R.; Koch, R. J.; Schaefer, J. A.; Kriscok, S. *Phys. Status Solidi B* **2010**, *247*, 1658.
(138) Noguchi, M.; Hirakawa, K.; Ikoma, T. *Surf. Sci.* **1992**, *271*, 260.
(139) Crowell, C. R.; Sze, S. M. *Solid-State Electron.* **1966**, *9*, 1035.
(140) von Wenckstern, H.; Kaidashev, E. M.; Lorenz, M.; Hochmuth, H.; Biehne, G.; Lenzner, J.; Gottschalch, V.; Pickenhain, R.; Grundmann, M. *Appl. Phys. Lett.* **2004**, *84*, 79.
(141) Leamy, H. J. *J. Appl. Phys.* **1982**, *53*, R51.
(142) Huang, H.-C. W.; Aliotta, C. F.; Ho, P. S. *Appl. Phys. Lett.* **1982**, *41*, 54.
(143) Zhu, S. Q.; Rau, E. I.; Yang, F.-H.; Zheng, H.-Z. *Chin. Phys. Lett.* **2002**, *19*, 1329.
(144) Gustafsson, A.; Björk, M. T.; Samuelson, L. *Nanotechnology* **2007**, *18*, No. 205306.
(145) Ahn, Y.; Dunning, J.; Park, J. *Nano Lett.* **2005**, *5*, 1367.
(146) Hiesgen, R.; Meissner, D. *J. Phys. Chem. B* **1998**, *102*, 6549.
(147) Kuk, Y.; Becker, R. S.; Silverman, P. J.; Kochanski, G. P. *Phys. Rev. Lett.* **1990**, *65*, 456.
(148) Ertl, G. *Angew. Chem., Int. Ed.* **1990**, *29*, 1219.
(149) Weisz, P. B. *J. Chem. Phys.* **1953**, *21*, 1531.
(150) Morrison, S. R. *The Chemical Physics of Surfaces*, 2 ed.; Plenum: New York, 1990.
(151) Weisz, P. B. *J. Chem. Phys.* **1952**, *20*, 1483.
(152) Batzill, M.; Diebold, U. *Prog. Surf. Sci.* **2005**, *79*, 47.
(153) Engler, C.; Lorenz, W. *Surf. Sci.* **1981**, *104*, 549.
(154) Lorenz, W.; Engler, C. *Surf. Sci.* **1982**, *114*, 607.
(155) Memming, R. *Prog. Surf. Sci.* **1985**, *17*, 7.
(156) Watson, D. F.; Meyer, G. J. *Annu. Rev. Phys. Chem.* **2005**, *56*, 119.
(157) Memming, R. *Surf. Sci.* **1980**, *101*, 551.
(158) Memming, R.; Schröppel, F.; Bringmann, U. *J. Electroanal. Chem.* **1979**, *100*, 307.
(159) Nakao, M.; Itoh, K.; Honda, K. *J. Phys. Chem.* **1984**, *88*, 4906.
(160) Hagfeld, A.; Grätzel, M. *Chem. Rev.* **1995**, *95*, 49.
(161) *Photocatalysis: Science and Technology*; Kaneko, M., Okura, I., Eds.; Springer-Verlag: New York, 2002.
(162) Albery, W. J.; Bartlett, P. N. *J. Electrochem. Soc.* **1984**, *131*, 315.
(163) *CRC Handbook of Chemistry and Physics*, 85th ed.; Lide, D. R., Ed.; CRC Press: Boca Raton, FL, 2005, pp 12.
(164) Yagi, E.; Hasiguti, R. P.; Aono, M. *Phys. Rev. B* **1996**, *54*, 7945.
(165) Schierbaum, K. D.; Weimar, U.; Göpel, W.; Kowalkowski, R. *Sens. Actuators, B* **1991**, *3*, 205.
(166) Franke, M. E.; Koplin, T. J.; Simon, U. *Small* **2006**, *2*, 36.
(167) Ohno, T.; Haga, D.; Fujihara, K.; Kaizaki, K.; Matsumura, M. *J. Phys. Chem. B* **1997**, *101*, 6415.
(168) Fujihara, K.; Izumi, S.; Ohno, T.; Matsumura, M. *J. Photochem. Photobiol. A* **2000**, *132*, 99.
(169) Ohnishi, T.; Nakato, Y.; Tsubomura, H. *Ber. Bunsen-Ges. Phys. Chem.* **1975**, *79*, 523.
(170) Kavan, l.; Grätzel, M.; Gilbert, S. E.; Klemenz, C.; Scheel, H. J. *J. Am. Chem. Soc.* **1996**, *118*, 6716.
(171) Zhang, Z.; Wang, C.-C.; Zakaria, R.; Ying, J. Y. *J. Phys. Chem. B* **1998**, *102*, 10871.
(172) Wang, Y.; Cheng, H.; Hao, Y.; Ma, J.; Li, W.; Cai, S. *Thin Solid Films* **1999**, *349*, 120.
(173) Xu, A.-W.; Gao, Y.; Liu, H. Q. *J. Catal.* **2002**, *207*, 151.
(174) Carp, O.; Huisman, C. L.; Reller, A. *Prog. Solid State Chem.* **2004**, *32*, 33.
(175) Choi, W.; Termin, A.; Hoffmann, M. R. *J. Phys. Chem.* **1994**, *98*, 13669.
(176) Quintana, M.; Edvinsson, T.; Hagfeldt, A.; Boschloo, G. *J. Phys. Chem. C* **2007**, *111*, 1035.
(177) Özgür, Ü.; Alivov, Y. I.; Liu, C.; Teke, A.; Reshchikov, M. A.; Doğan, S.; Avrutin, V.; Cho, S.-J.; Morkoç, H. *J. Appl. Phys.* **2005**, *98*, No. 041301.
(178) Mikheeva, E. P. *Russ. Chem. Rev.* **1989**, *58*, 881.
(179) Pacchioni, G.; Lomas, J. R.; Illas, F. *J. Mol. Catal. A: Chem.* **1997**, *119*, 263.
(180) Deshlahra, P.; Schneide, W. F.; Bernstein, G. H.; Wolf, E. E. *J. Am. Chem. Soc.* **2011**, *133*, 16459.
(181) Zeng, Y.; Cheng, G. F.; Wen, M.; Wu, W. *Prog. Org. Coat.* **2008**, *61*, 321.
(182) Zeng, Y.; Liu, J. T.; Wu, W.; Wang, J. R.; Lee, S. W. *Ceram. Int.* **2008**, *34*, 351.
(183) He, C.; Xiong, Y.; Zhu, X. H. *Thin Solid Films* **2002**, *422*, 235.
(184) Brinkley, D.; Engel, T. *J. Phys. Chem. B* **2000**, *104*, 9836.
(185) Li, M.; Hebenstreit, W.; Gross, L.; Diebold, U.; Henderson, M. A.; Jennison, D. R.; Schultz, P. A.; Sears, M. P. *Surf. Sci.* **1999**, *437*, 173.
(186) Li, M.; Hebenstreit, W.; Diebold, U.; Tyryshkin, A. M.; Bowman, M. K.; Dunham, G. G.; Henderson, M. A. *J. Phys. Chem. B* **2000**, *104*, 4944.
(187) Smith, R. D.; Bennett, R. A.; Bowker, M. *Phys. Rev. B* **2002**, *66*, No. 035409.
(188) Park, K. T.; Pan, M.; Meunier, V.; Plummer, E. W. *Phys. Rev. B* **2007**, *75*, No. 245415.
(189) Tao, J. G.; Luttrell, T.; Batzill, M. *Nat. Chem.* **2011**, *3*, 296.
(190) Wilson, J. N.; Idriss, H. *J. Catal.* **2003**, *214*, 46.
(191) Wilson, J. N.; Idriss, H. *J. Am. Chem. Soc.* **2002**, *124*, 11284.
(192) Grätzel, M. *Heterogeneous Photochemical Electron Transfer*; CRC Press: Boca Raton, FL, 1988.
(193) Liu, G.; Yu, J. C.; Lu, G. Q.; Cheng, H. M. *Chem. Commun.* **2011**, *47*, 6763.
(194) Pan, J.; Liu, G.; Lu, G. Q.; Cheng, H. M. *Angew. Chem., Int. Ed.* **2011**, *50*, 2133.
(195) D'Arienzo, M.; Carbajo, J.; Bahamonde, A.; Crippa, M.; Polizzi, S.; Scotti, R.; Wahba, L.; Morazzoni.. *J. Am. Chem. Soc.* **2011**, *133*, 17652.
(196) Farneth, W. E.; McLean, R. S.; Bolt, J. D.; Dokou, E.; Barteau, M. A. *Langmuir* **1999**, *15*, 8569.
(197) Ohsawa, T.; Henderson, M. A.; Chambers, S. A. *J. Phys. Chem. C* **2010**, *114*, 6595.
(198) Zhou, X.; Lan, J.; Liu, G.; Deng, K.; Yang, Y.; Nie, G.; Yu, J.; Zhi, L. *Angew. Chem., Int. Ed.* **2012**, *51*, 178.
(199) Kislov, N.; Lahiri, J.; Verma, H.; Goswami, D. Y.; Stefanakos, E.; Batzill, M. *Langmuir* **2009**, *25*, 3310.
(200) Matsumoto, Y.; Ohsawa, T.; Takahashi, R.; Koinuma, H. *Thin Solid Films* **2005**, *486*, 11.
(201) Hotsenpiller, P. A. M.; Bolt, J. D.; Farneth, W. E.; Lowekamp, J. B.; Rohrer, G. S. *J. Phys. Chem. B* **1998**, *102*, 3216.
(202) Giocondi, J. L.; Salvador, P. A.; Rohrer, G. S. *Top. Catal.* **2007**, *44*, 529.
(203) Giocondi, J. L.; Rohrer, G. S. *Top. Catal.* **2008**, *49*, 18.
(204) Giocondi, J. L.; Rohrer, G. S. *J. Phys. Chem. B* **2001**, *105*, 8275.
(205) Kalinin, S. V.; Bonnell, D. A.; Alvarez, T.; Lei, X.; Hu, Z.; Ferris, J. H.; Zhang, Q.; Dunn, S. *Nano Lett.* **2002**, *2*, 589.
(206) Giocondi, J. L.; Rohrer, G. S. *J. Am. Ceram. Soc.* **2003**, *86*, 1182.
(207) Burbure, N. V.; Salvador, P. A.; Rohrer, G. S. *J. Am. Ceram. Soc.* **2006**, *89*, 2943.
(208) Schultz, A. M.; Zhang, Y. L.; Salvador, P. A.; Rohrer, G. S. *ACS Appl. Mater. Interfaces* **2011**, *3*, 1562.
(209) Dunn, S.; Jones, P. M.; Gallardo, D. E. *J. Am. Chem. Soc.* **2007**, *129*, 8724.
(210) Parker, R. A. *Phys. Rev. B* **1961**, *124*, 1719.
(211) Brody, P. S. *Solid State Commun.* **1973**, *12*, 673.
(212) Brody, P. S. *J. Solid State Chem.* **1975**, *12*, 193.
(213) Fridkin, V. M. *Ferroelectrics* **1984**, *53*, 169.
(214) Zhao, J.; Yang, J. L.; Petek, H. *Phys. Rev. B* **2009**, *80*, 235416.
(215) Onishi, H.; Aruga, T.; Egawa, C.; Iwasawa, Y. *Surf. Sci.* **1988**, *193*, 33.

(216) Román, E. L.; de Segovia, J.; Kurtz, R. L.; Stockbauer, R.; Madey, T. *Surf. Sci.* **1992**, *273*, 40.
(217) Berger, T.; Sterrer, M.; Diwald, O.; Knözinger, E. *ChemPhysChem* **2005**, *6*, 2104.
(218) Furube, A.; Asahi, T.; Masuhara, H.; Yamashita, H.; Anpo, M. *J. Phys. Chem. B* **1999**, *103*, 3120.
(219) Hiehata, K.; Sasahara, A.; Onishi, H. *Jpn. J. Appl. Phys.* **2008**, *118*, 5098.
(220) de Lara-Castells, M. P.; Krause, J. L. *J. Chem. Phys.* **2001**, *115*, 4798.
(221) de Lara-Castells, M. P.; Krause, J. L. *Chem. Phys. Lett.* **2002**, *354*, 483.
(222) Anpo, M.; Che, M.; Fubini, B.; Garrone, E.; Giamello, E.; Paganini, M. C. *Top. Catal.* **1999**, *8*, 189.
(223) Henderson, M. A.; Epling, W. S.; Perkins, C. L.; Peden, C. H. F.; Diebold, U. *J. Phys. Chem. B* **1999**, *103*, 5328.
(224) Topping, J. *Proc. R. Soc. London, Ser. A* **1927**, *114*, 67.
(225) Macdonald, J. R.; Barlow, C. A., Jr. *J. Chem. Phys.* **1963**, *39*, 412.
(226) Uetsuka, H.; Pang, C.; Sasahara, A.; Onishi, H. *Langmuir* **2005**, *21*, 11802.
(227) Sasahara, A.; Pang, C. L.; Onishi, H. *J. Phys. Chem. B* **2006**, *110*, 13453.
(228) Okazaki, K.; Morikawa, Y.; Tanaka, S.; Tanaka, K.; Kohyama, M. *Phys. Rev. B* **2004**, *69*, No. 235404.
(229) Laursen, S.; Linic, S. *J. Phys. Chem. C* **2009**, *113*, 6689.
(230) Knight, M. W.; Sobhani, H.; Nordlander, P.; Halas, N. J. *Science* **2011**, *332*, 702.
(231) Lee, Y. K.; Jung, C. H.; Park, J.; Seo, H.; Somorjai, G. A.; Park, J. Y. *Nano Lett.* **2011**, *11*, 4251.
(232) Rycenga, M.; Cobley, C. M.; Zeng, J.; Li, W. Y.; Moran, C. H.; Zhang, Q.; Qin, D.; Xia, Y. N. *Chem. Rev.* **2011**, *111*, 3669.
(233) Xia, Y. N.; Xiong, Y. J.; Lim, B.; Skrabalak, S. E. *Angew. Chem., Int. Ed.* **2009**, *48*, 60.
(234) Peng, S.; McMahon, J. M.; Schatz, G. C.; Gray, S. K.; Sun, Y. G. *Proc. Natl. Acad. Sci. U.S.A.* **2010**, *107*, 14530.
(235) Tian, Y.; Tatsuma, T. *J. Am. Chem. Soc.* **2005**, *127*, 7632.
(236) Silva, C. G.; Juárez, R.; Marino, T.; Molinari, R.; García, H. *J. Am. Chem. Soc.* **2011**, *133*, 595.
(237) Kowalska, E.; Mahaney, O. O. P.; Abe, R.; Ohtani, B. *Phys. Chem. Chem. Phys.* **2010**, *12*, 2344.
(238) Primo, A.; Marino, T.; Corma, A.; Molinari, R.; García, H. *J. Am. Chem. Soc.* **2011**, *133*, 6930.
(239) Kochuveedu, S. T.; Kim, D.-P.; Kim, D. H. *J. Phys. Chem. C* **2012**, *116*, 2500.
(240) Bickley, R. I.; Gonzalez-Carreno, T.; Lees, J. S.; Palmisano, L.; Tilley, R. J. D. *J. Solid State Chem.* **1991**, *92*, 178.
(241) Su, R.; Beschstein, R.; Sø, L.; Vang, R. T.; Sillassen, M.; Esbjörnsson, B.; Palmqvist, A.; Besenbacher, F. *J. Phys. Chem. C* **2011**, *115*, 24287.
(242) Jafry, H. R.; Liga, M. V.; Li, Q. L.; Barron, A. R. *Environ. Sci. Technol.* **2011**, *45*, 1563.
(243) Leung, D. Y. C.; Fu, X. L.; Wang, C. F.; Ni, M.; Leung, M. K. H.; Wang, X. X.; Fu, X. Z. *ChemSusChem* **2010**, *3*, 681.
(244) Sun, B.; Vorontsov, A. V.; Smirniotis, P. G. *Langmuir* **2003**, *19*, 3151.
(245) Nair, R. G.; Paul, S.; Samdarshi, S. K. *Sol. Energy Mater. Sol. Cells* **2011**, *95*, 1901.
(246) Zachariah, A.; Baiju, K. V.; Shukla, S.; Deepa, K. S.; James, J.; Warrier, K. G. K. *J. Phys. Chem. C* **2008**, *112*, 11345.
(247) Baiju, K. V.; Zachariah, A.; Shukla, S.; Biju, S.; Reddy, M. L. P.; Warrier, K. G. K. *Catal. Lett.* **2009**, *130*, 130.
(248) Kho, Y. K.; Iwase, A.; Teoh, W. Y.; Mädler, L.; Kudo, A.; Amal, R. *J. Phys. Chem. C* **2010**, *114*, 2821.
(249) Zhang, X. R.; Lin, Y. H.; He, D. Q.; ZHang, J. F.; Fan, J. F.; Xie, T. F. *Chem. Phys. Lett.* **2011**, *504*, 71.
(250) Xiong, G.; Shao, R.; Droubay, T. C.; Joly, A. G.; Beck, K. M.; Chambers, S. A.; Hess, W. P. *Adv. Funct. Mater.* **2007**, *17*, 2133.
(251) Kawahara, T.; Konishi, Y.; Tada, H.; Tohge, N.; Nishii, J.; Ito, S. *Angew. Chem., Int. Ed.* **2002**, *41*, 2811.
(252) Wei, D.; Amaratunga, G. *Int. J. Electrochem. Sci.* **2007**, *2*, 897.
(253) Gerischer, H. *J. Phys. Chem.* **1984**, *88*, 6096.
(254) Zhang, N.; Liu, S. Q.; Fu, X. Z.; Xu, Y. J. *J. Phys. Chem. C* **2011**, *115*, 9136.
(255) Hirakawa, T.; Kamat, P. V. *J. Am. Chem. Soc.* **2005**, *127*, 3928.
(256) Hirakawa, T.; Kamat, P. V. *Langmuir* **2004**, *20*, 5645.